Functioning Water-Insoluble Ferrocenes for Aqueous Organic Flow Battery via Host–Guest Inclusion

Yuanyuan Li[+],[a] Ziang Xu[+],[b, d] Yahua Liu,[a] Shijian Jin,[c] Eric M. Fell,[b] Baoguo Wang,[d] Roy G. Gordon,[c] Michael J. Aziz,[b] Zhengjin Yang,*[a, e] and Tongwen Xu*[a]

Ferrocene (Fc) is one of the very limited organic catholyte options for aqueous organic flow batteries (AOFBs), a potential electrochemical energy storage solution to the intermittency of renewable electricity. Commercially available Fc derivatives are barely soluble in water, while existing methods for making water-soluble Fc derivatives by appending hydrophilic or charged moieties are tedious and time-consuming, with low yields. Here, a strategy was developed based on host–guest inclusion to acquire water-soluble Fc-based catholytes by simply mixing Fc derivatives with β-cyclodextrins (β-CDs) in water. Factors determining the stability and the electrochemical behavior of the inclusion complexes were identified. When adopted in a neutral pH AOFB, the origin of capacity loss was identified to be a chemical degradation caused by the nucleophilic attack on the center Fe^{III} atom of the oxidized Fc derivatives. By limiting the state of charge, a low capacity fade rate of 0.0073% h^{-1} (or 0.0020% per cycle) was achieved. The proposed strategy may be extended to other families of electrochemically active water-insoluble organic compounds, bringing more electrolyte options for practical AOFB applications.

Introduction

With the rapidly falling cost of renewable energy sources, they may partially satisfy global energy demand and have great potential in addressing environmental challenges.[1] However, the intermittency of these renewable energy sources has to be mitigated through approaches such as effective and affordable energy storage technologies, thereby realizing grid-scale adoption.[2] Aqueous organic flow battery (AOFB) that exploits the reversible electrochemical reaction of organic compounds in water is deemed as a potentially viable energy storage technology by virtue of its low cost, improved safety and easy scale-up.[3]

An AOFB consists of organic compounds with high redox potential for the positive side (catholyte) and organic counterparts with low redox potential for the negative side (anolyte). Although great success has been achieved for the anolyte, with an extremely low capacity fade rate of $\leq$0.02% per day demonstrated,[3b,4] the few options for the organic catholyte include functionalized benzoquinones,[5] radialene dianions,[6] ferrocene[7] and 2,2,6,6-tetramethylpiperidine-1-oxyl (TEMPO) derivatives.[8] Benzoquinones have been operated under highly acidic solutions and exhibit poor stability due to side reactions.[9] Radialene dianions are chemically unstable and poorly soluble in water.[6] Ferrocene and TEMPO derivatives are the best-performing organic catholyte options, but their performance to date does not merit commercialization.[3b]

A challenging task is the hydrophilic functionalization of ferrocene and TEMPO derivatives for enhanced water solubility, as most of them are barely soluble in water. By attaching quaternary ammonium or sulfonate groups to the ferrocene core, water-soluble ferrocene-based catholytes, such as ferrocenylmethyl)trimethylammonium chloride (FcNCl),[7a] N^1-ferrocenylmethyl-N^1,N^1,N^2,N^2,N^2-pentamethylpropane-1,2-diaminium dibromide (FcN_2Br_2),[7a] bis((3-trimethylammonio)propyl) ferrocene (BTMAP-Fc)[7b] and ferrocene bis(propyl sodiumsulfite) (Fc-SO_3Na),[7c] were prepared. A similar strategy was employed for making water-soluble TEMPO-based catholytes, affording 4-hydroxy-TEMPO (4-HO-TEMPO),[8a] *N*,*N*,*N*-2,2,6,6-heptamethylpiperidinyl oxy-4-ammonium chloride (TEMPTMA),[8b] glycidyltrimethylammonium cation-grafted TEMPO (g^+-TEMPO),[8c] TEMPO-4-sulfate potassium salt (TEMPO-4-SO_3K),[8d] and 4-[3-(trimethylammonio)propoxy]-TEMPO (TMAP-TEMPO).[8e] Nevertheless, these molecular engineering methods are time-consuming and require multiple steps of organic synthesis, with

[a] Y. Li,[+] Y. Liu, Prof. Z. Yang, Prof. T. Xu
CAS Key Laboratory of Soft Matter Chemistry
iChEM (Collaborative Innovation Center of Chemistry for Energy Materials)
School of Chemistry and Material Science
University of Science and Technology of China
Hefei 230026 (P. R. China)
E-mail: yangzj09@ustc.edu.cn
twxu@ustc.edu.cn
[b] Z. Xu,[+] E. M. Fell, Prof. M. J. Aziz
Harvard John A. Paulson School of Engineering and Applied Sciences
29 Oxford Street, Cambridge, Massachusetts 02138 (USA)
[c] S. Jin, Prof. R. G. Gordon
Department of Chemistry and Chemical Biology
Harvard University
12 Oxford Street, Cambridge, Massachusetts, 02138 (USA)
[d] Z. Xu,[+] Prof. B. Wang
The State Key Laboratory of Chemical Engineering
Department of Chemical Engineering
Tsinghua University
Beijing 100084 (P. R. China)
[e] Prof. Z. Yang
Dalian National Laboratory for Clean Energy
Dalian 116023 (P. R. China)
[+] These authors contributed equally to this work.

Supporting information for this article is available on the WWW under https://doi.org/10.1002/cssc.202002516

low yields. For instance, the synthesis of TEMPTMA consists of four steps, or three steps in an optimized route.[8b] The synthesis of BTMAP-Fc was completed in three steps (two of them were conducted at 0 °C), with a yield of approximately 50%,[7b] while the synthesis of TMAP-TEMPO has two steps, with an overall yield of $<25\%$.[8e] Therefore, it is important to explore alternative strategies that lead to water-soluble catholyte, averting sophisticated organic syntheses.

Hereby we present a host–guest inclusion strategy that can make water-insoluble organic compounds water-soluble, as exemplified with ferrocene derivatives and β-cyclodextrins (β-CDs), a class of macrocyclic oligosaccharides with hydrophobic inner cavity and hydrophilic outer rim that enable water solubility.[10] Driven by hydrophobic interactions, the hydrophobic ferrocene derivatives can enter the inner cavity of β-CDs, forming host–guest inclusion complexes.[11]

By mixing ferrocene derivatives with β-CDs, such as hydroxypropyl-β-cyclodextrin (HP-β-CD), in water at room temperature, water-soluble inclusion complexes, such as Fc⊂-HP-β-CD, HEFc⊂HP-β-CD and HMFc⊂HP-β-CD were obtained. They exhibited high redox potential of 0.5 V vs. SHE (standard hydrogen electrode) at neutral pH, low electron transfer resistance of 0.2 $\Omega\,cm^2$, fast redox kinetics of 10^{-2} $cm\,s^{-1}$, and comparable chemical stability to the parent ferrocene derivatives. We identified the factors that would influence the binding between ferrocene derivatives and β-CDs and explored how the inclusion complexes behaved in electrochemical reactions.

When paired with bis(3-trimethylammonio)propyl viologen tetrachloride (BTMAP–Vi) anolyte,[7b] the battery demonstrated an open-circuit voltage of approximately 0.9 V and a capacity fade rate of 0.10% h^{-1} (or 0.041% per cycle). We investigated in detail capacity loss caused by the decomposition of the inclusion complexes, which is attributed mainly to the nucleophilic attack on ferrocenium ions. By limiting the state of charge (SOC), the degradation of ferrocenium ions was mitigated and the improved cycling stability with a capacity fade rate of 0.0073% h^{-1} (or 0.0020% per cycle) was demonstrated.

Results and Discussion

Inclusion of guest ferrocene derivatives in host β-CDs

The host–guest interaction between β-CDs and ferrocene derivatives enables the formation of inclusion complexes that are water-soluble. β-CDs are selected as they have the strongest binding ability with ferrocene derivatives,[11] and highly water-soluble β-CDs, such as methylated β-CD (M-β-CD) and hydroxypropylated β-CD (HP-β-CD), can be obtained through alkyl substitution on hydroxy groups.[10] Commercially available ferrocene derivatives, including Fc, hydroxymethylferrocene (HMFc), 1-hydroxyethylferrocene (HEFc), carboxylferrocene (CFc), and acetylferrocene (Afc) were selected to study the inclusion complexes of ferrocene derivatives and β-CDs (Figure 1a). The inclusion complexes were prepared by simply mixing them in water. An intriguing phenomenon we observed in the experiment is the change in water solubility; ferrocene itself is barely water-soluble, while a homogenous solution was formed as we added three portions of HP-β-CD to the mixture (Figure 1b).

The dissolution of Fc in water when HP-β-CD was added is due to the formation of host–guest inclusion complexes, rather than surfactant effect. This was proved by two-dimensional NMR spectroscopy, namely nuclear Overhauser effect spectroscopy (NOESY) and diffusion ordered spectroscopy (DOSY). The ^1H–^1H space correlation between Fc and HP-β-CD was observed in the NOESY spectrum (Figure 1c) and there is only one diffusion signal (except the diffusion signal of D_2O) in the DOSY spectrum, implying they move as a single molecule (Figure 1d). Similar results were obtained for HMFc and HEFc (Figure S1).

Stability of the inclusion complexes is, however, significantly affected by the structure of ferrocene derivatives. For instance, AFc and CFc cannot form stable host–guest inclusion complexes with HP-β-CD even after a long time of agitation (Figure 1e, Figure S2). This can be explained from the viewpoint of hydrophobic interactions between ferrocene derivatives and HP-β-CD. The driving force for the formation of inclusion complexes is hydrophobic interactions[11b] and varies with the polarity of the ferrocene derivatives. Our density functional theory (DFT) calculations[12] on dipole moments of ferrocene derivatives show CFc and AFc have much higher polarity than the others (Table S1). The increase in polarity weakens the interaction between CFc/AFc molecules and the non-polar inner cavity of HP-β-CD. The binding strength was further investigated by isothermal titration calorimetry (ITC) measurements (Figure S3, and Table S2). The results reveal that as the polarity of the ferrocene derivatives decreases, the binding between ferrocene derivatives and HP-β-CD become stronger, as reflected by a more negative molar Gibbs free-energy change ($\triangle G$) and a larger formation constant (K), which is in the range of 10^3–10^4 M^{-1} (Figure 1f).

Similar results were obtained for β-CD and M-β-CD (Figures S4 and S5, Table S2), which were, however, not further investigated due to low solubility of β-CD and high cost of M-β-CD, respectively (Table S3). The solubility of ferrocene in water enabled by its inclusion in HP-β-CD was determined to be 0.28 M. At higher concentrations, the solutions are too viscous to be pumped.

Electrochemical properties of ferrocene inclusion complexes

Electrochemical measurements show that the as-formed inclusion complexes inherit the redox activity from the ferrocene derivatives but undergo a slightly different electrode reaction mechanism. The electrode reaction can be described by a chemical–electrochemical (CE) redox mechanism, as the direct oxidation of the inclusion complexes is thermodynamically and kinetically difficult.[13] The inclusion complexes first dissociate and the ferrocene derivatives, in the free form, are then electrochemically oxidized on the electrode. The oxidation product, ferrocenium ions, does not combine, or weakly combine, with HP-β-CD (Figure 2a). The following observations are fully consistent with this mechanism.

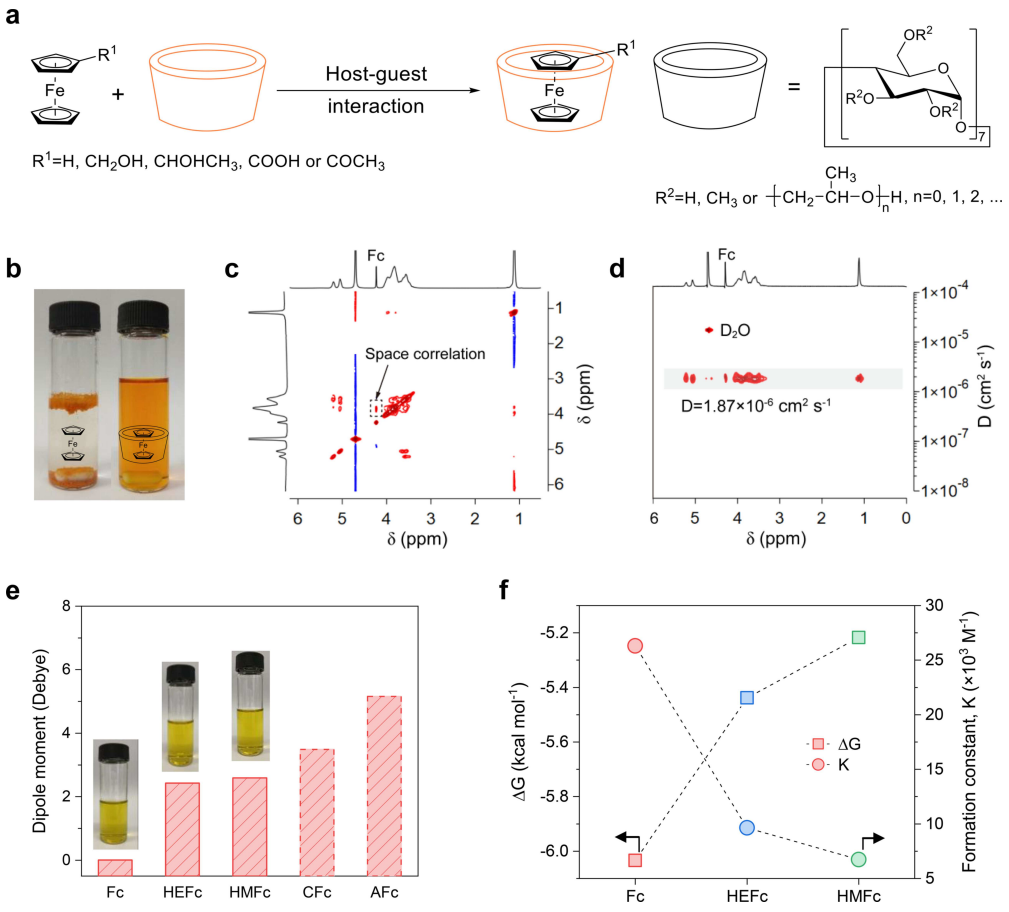

Figure 1. Inclusion of guest ferrocene derivatives in host β-CDs. (a) Illustration showing the host–guest inclusion of ferrocene derivatives in β-CDs. The driving force for the host–guest inclusion is hydrophobic interaction. (b) Photos of Fc in water in the absence (left) and in the presence (right) of HP-β-CD. Two-dimensional NOESY (c) and DOSY (d) spectra showing the intermolecular interaction between Fc and HP-β-CD. The dashed box highlights the interaction peak and *D* is the diffusion coefficient, as determined from the DOSY spectrum. (e) Dipole moment of ferrocene derivatives. Inset photos show the stable solutions of the inclusion complexes. Solutions for CFc and AFc can be found in the Supporting Information and precipitations form over time. (f) Molar change of Gibbs free energy (△*G*) and formation constant (*K*) characterizing the formation of the inclusion complexes.

Cyclic voltammograms recorded at low potential sweeping rate give a ratio of cathodic to anodic peak current, that is, $i_{p,c}/i_{p,a}$, close to unity. As the potential sweeping rate increases, the anodic peaks flatten (Figure S6) and the $i_{p,c}/i_{p,a}$ ratio increases. A high $i_{p,c}/i_{p,a}$ ratio of 1.8 was observed for HMFc⊂HP-β-CD at 5 $V s^{-1}$. This value becomes greater, as the binding strength between ferrocene derivatives and HP-β-CD gets stronger, as reflected by the increase in formation constant, *K*. Fc⊂HP-β-CD that has the largest *K* value gives the highest $i_{p,c}/i_{p,a}$ ratio of 2.4 (Figure 2b). High *K* values indicate slow dissociation of ferrocene derivatives from the inclusion complexes, thereby leading to small anodic peak current and big $i_{p,c}/i_{p,a}$ ratio.

The small formation constants (*K'*) between ferrocenium ions and HP-β-CD, as determined from the thermodynamic calculation employing peak potentials in cyclic voltammograms (see Supporting Information), imply that ferrocenium (Fc^+) weakly combines with HP-β-CD ($K' = 794.2\ M^{-1}$), while $HEFc^+$ and $HMFc^+$ do not ($K' = 0.85$ and $1.28\ M^{-1}$, respectively, Figure 2c, Table S4). The absence of protection from HP-β-CD suggests that ferrocenium ions are still susceptible to the known nucleophilic attacks of water.[14]

The dissociation-complexation equilibrium of the inclusion complexes results in positively shifted potentials compared to the parent ferrocene derivatives, as determined from cyclic voltammetry (CV) studies at 50 $mV s^{-1}$. As more HP-β-CD was added, the equilibrium is shifted to the left (Figure 2a, top row), making ferrocene derivatives hard to oxidize, resulting in increased oxidation potentials. The increase turns less obvious when three portions of HP-β-CD were added (Figure S7 and S8). This can be ascribed to the strong binding (big formation constant) of the inclusion complexes. At a molar ratio of 1:3, Fc⊂HP-β-CD, HEFc⊂HP-β-CD and HMFc⊂HP-β-CD delivered reversible oxidation peaks are at 0.50, 0.53 and 0.52 V vs. SHE, respectively (Figure 2d, Figure S9).

Rotating disk electrode (RDE) measurements (Figures S10, S11 and S12) revealed a diffusion-controlled oxidation process and the diffusion coefficients (*D*) of Fc⊂HP-β-CD, HEFc⊂HP-β-CD and HMFc⊂HP-β-CD were calculated to be 1.87×10^{-6}, 2.12×10^{-6} and 2.22×10^{-6} $cm^2 s^{-1}$, respectively. The values are slightly lower than those reported for ferrocene-based electrolyte molecules,[7] considering the higher molecular weight of the inclusion complexes (Figure 2e). The *D* values are in good

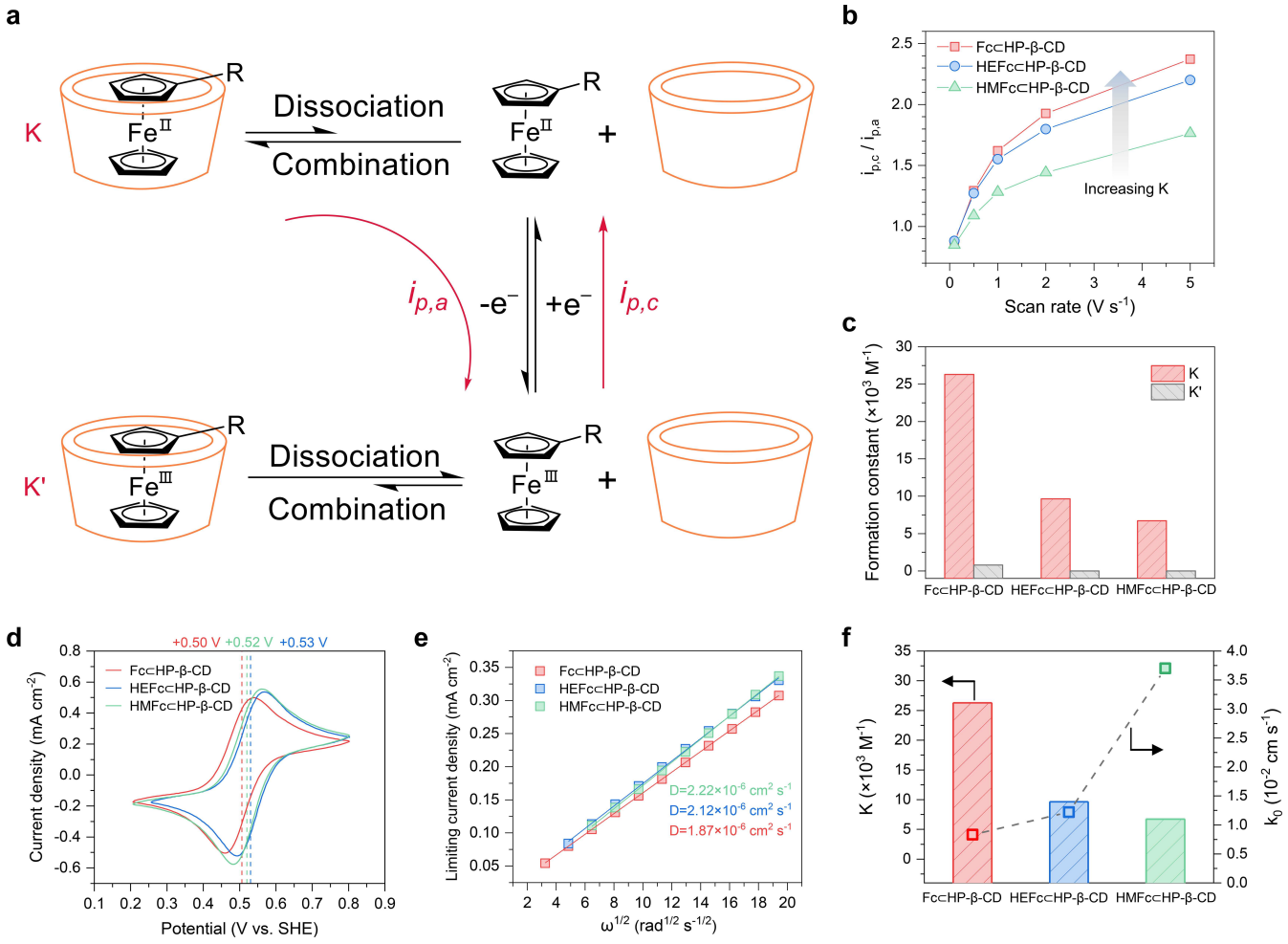

Figure 2. Electrochemical properties of ferrocene inclusion complexes. (a) Illustrations showing the electrochemical oxidation and reduction of ferrocene inclusion complexes. The shorter and longer half-arrows represent the reaction is thermodynamically unfavorable and favorable, respectively. (b) The ratio of $i_{p,c}/i_{p,a}$ as a function of potential sweeping rate in CV measurements; $i_{p,c}$ *and* $i_{p,a}$ are the cathodic and anodic peak current, respectively. The inclusion complex electrolytes were tested under 10 mM ferrocene derivative and 30 mM HP-β-CD in 1 M NaCl solution. (c) Formation constants of Fc, HEFc, and HMFc with HP-β-CD in the reduced form (*K*) and the oxidized form (*K'*). (d) Cyclic voltammograms of 10 mM Fc⊂HP-β-CD, HMFc⊂HP-β-CD, and HEFc⊂HP-β-CD (1:3) in 1 M NaCl solution recorded at 50 mV s^{-1}. (e) Levich plots of the limiting current density versus the square root of rotating speed in RDE measurements for 1 mM Fc⊂HP-β-CD, HMFc⊂HP-β-CD, and HEFc⊂HP-β-CD (1:3) in 1 M NaCl solution. (f) Kinetic rate constant (k_0) versus formation constant (*K*) of ferrocene inclusion complexes.

accordance with those determined from DOSY spectra (Figure 1d, Figure S1). The oxidation rate constants (k_0) are 8.31×10^{-3}, 1.22×10^{-2} and 3.70×10^{-2} cm s^{-1} for Fc⊂HP-β-CD, HEFc⊂-HP-β-CD and HMFc⊂HP-β-CD, respectively, orders of magnitude higher than those of FcNCl and FcN_2Br_2 (Table S5).[7a] Note that k_0 is inversely related to the formation constants (Figure 2f), implying the preceding dissociation slows the redox kinetics of the inclusion complexes.

Performance of the pH-neutral AOFBs assembled with ferrocene inclusion complexes

The water solubility and appropriate electrochemical properties render these inclusion complexes suitable for pH-neutral AOFBs. As a proof of concept, we constructed pH-neutral AOFBs with either Fc⊂HP-β-CD, HEFc⊂HP-β-CD or HMFc⊂HP-β-CD for the catholyte, and BTMAP-Vi, which was proved extremely stable, for the anolyte.[7b,15] The anolyte solutions were in excess amount to prevent potential side-reactions incurred cell imbalance. To prevent cross-contamination, a Selemion DSV anion-exchange membrane was sandwiched between the electrodes (Figure 3a).

The as-assembled Fc⊂HP-β-CD/BTMAP-Vi, HEFc⊂HP-β-CD/BTMAP-Vi and HMFc⊂HP-β-CD/BTMAP-Vi cells delivered open-circuit voltages (OCV) of 0.86, 0.89 and 0.88 V at 50% SOC, respectively (Figures S13, S14, and S15). The values are consistent with what we expected from CV studies (Figure 3b) and are 15% higher than the OCV of BTMAP-Fc/BTMAP-Vi (0.748 V).[7b] Polarizations of these cells were conducted at varied SOCs via linear sweep voltammetry (LSV). The highest peak power density obtained at approximately 100% SOC for Fc⊂HP-β-CD/BTMAP-Vi, HEFc⊂HP-β-CD/BTMAP-Vi and HMFc⊂HP-β-CD/

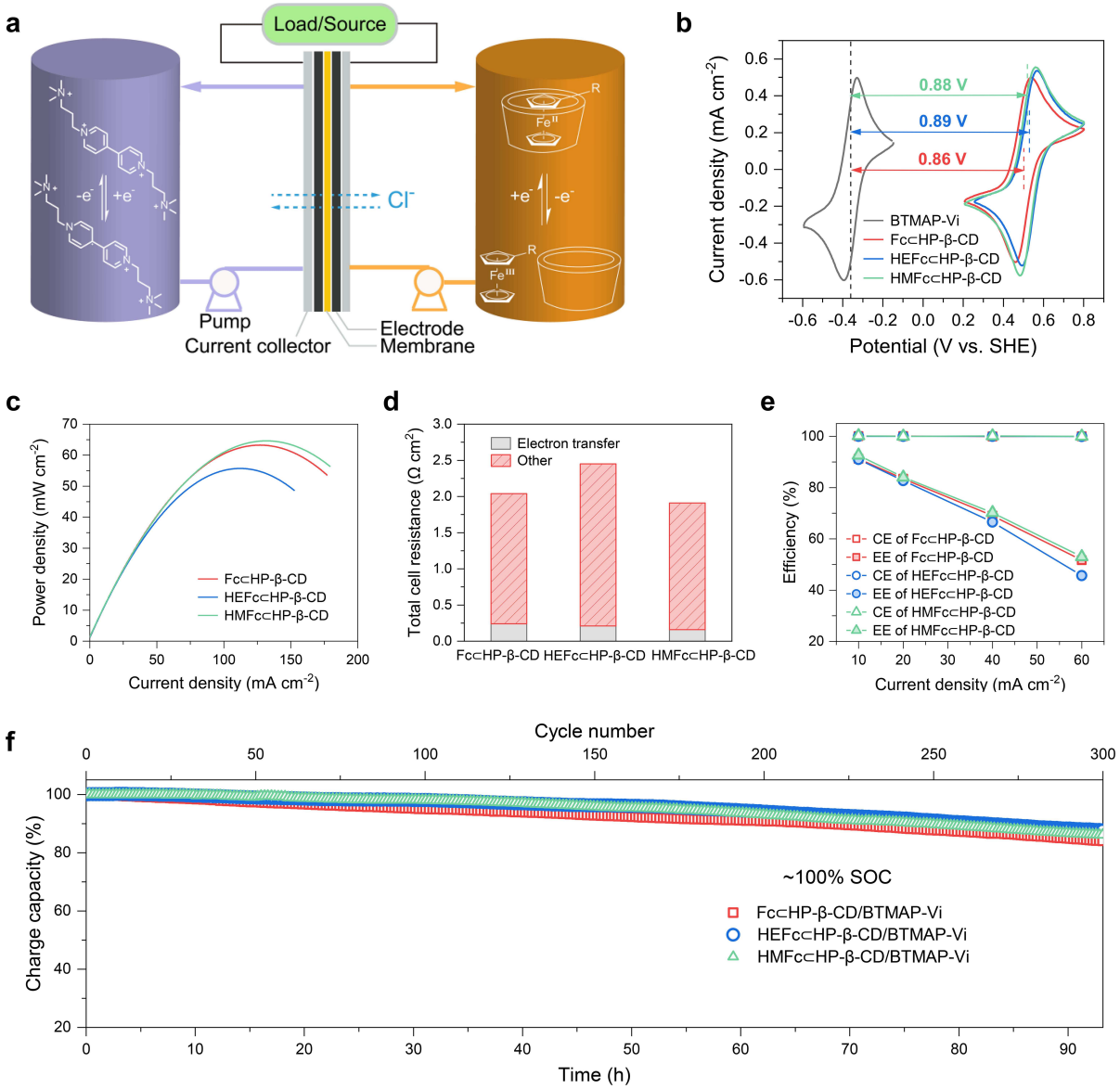

Figure 3. Performance of the pH-neutral AOFBs assembled with FcCHP-β-CD, HEFcCHP-β-CD or HMFcCHP-β-CD, when paired with BTMAP-Vi. (a) Schematic illustration showing the pH-neutral AOFBs. (b) Theoretical open-circuit-voltages of the pH-neutral AOFBs, as determined from the cyclic voltammograms of BTMAP-Vi, FcCHP-β-CD, HEFcCHP-β-CD, and HMFcCHP-β-CD. (c) Power density as a function of current density at approximately 100% SOC for the pH-neutral AOFBs. The catholyte comprised 10 mL of 0.1 M FcCHP-β-CD, HEFcCHP-β-CD or HMFcCHP-β-CD (1:3) in 1 M NaCl solution, and the anolyte comprised 15 mL of 0.1 M BTMAP–Vi in 1 M NaCl solution. (d) Total cell resistance and electron transfer resistance from cathode reactions. (e) Coulombic efficiency (CE) and energy efficiency (EE) as functions of cycling current density. At each current density, 5 repeated cycles were performed. (f) Long-term galvanostatic cycling of the as-assembled pH-neutral AOFBs at 40 mA cm^{-2} with potentiostatic hold at the end of every charge and discharge process for 300 consecutive cycles. The cutoff voltages for charge and discharge are 0.3 and 1.1 V, respectively. For better comparison, the initial capacity was arbitrarily defined as 100%.

BTMAP-Vi cells were 66.22, 58.16, and 68.55 mW cm^{-2}, respectively (Figure 3c).

Electrochemical impedance spectroscopy (EIS) analyses were conducted and the equivalent circuits were built (Figures S16, S17), giving a charge-transfer resistance (R_{ct}) of 0.24, 0.21, and 0.16 Ω cm^2 for FcCHP-β-CD, HEFcCHP-β-CD and HMFcCHP-β-CD, respectively. The difference in cathode R_{ct} can be ascribed to the different redox kinetics. However, R_{ct} accounts for only a small proportion (<11.8%) of the total cell resistance (as derived from polarization curves at 10% SOC) and therefore would not dramatically alter the peak power density of the cells (Figure 3d, Table S6). Membrane resistance contributes to more than 66.1% of the total area specific resistance (Table S6). An improved membrane with lower resistance will increase the power density.

Rate performance of FcCHP-β-CD/BTMAP-Vi, HEFcCHP-β-CD/BTMAP-Vi and HMFcCHP-β-CD/BTMAP-Vi was evaluated at constant current densities of 10, 20, 40, and 60 mA cm^{-2}. A coulombic efficiency of approximately 100% was observed at each current density for all the cells, while energy efficiency decreased with the increase in current densities. The energy efficiency for FcCHP-β-CD/BTMAP–Vi decreased from more

than 91% at 10 mA cm^{-2} to 51% at 60 mA cm^{-2} (Figure 3e), which can be ascribed to the greater ohmic polarization at higher current densities. Similar results were obtained for HEFc⊂HP-β-CD/BTMAP-Vi and HMFc⊂HP-β-CD/BTMAP-Vi, although the decrease in energy efficiency is more obvious for HEFc⊂HP-β-CD/BTMAP-Vi at high current density.

To evaluate the stability of Fc⊂HP-β-CD, HEFc⊂HP-β-CD and HMFc⊂HP-β-CD in cell cycling, extended galvanostatic cycling was conducted at 40 mA cm^{-2} by applying potential hold at the end of every charge and discharge process until the current density dropped to 4 mA cm^{-2} for 300 cycles. Results reveal total capacity loss rates of 0.053, 0.041 and 0.046% per cycle, or a temporal capacity fate rate of 0.17, 0.10 and 0.11% h^{-1} for Fc⊂HP-β-CD/BTMAP-Vi, HEFc⊂HP-β-CD/BTMAP-Vi and HMFc⊂HP-β-CD/BTMAP-Vi, respectively (Figure 3f).

Chemical stability analysis for ferrocene inclusion complexes

We attribute the total capacity loss to catholyte crossover and chemical degradation. The contribution of the catholyte crossover was estimated via post-mortem analysis of the anolyte by quantifying the amount of ferrocene derivatives with inductively coupled plasma-optical emission spectrometry (ICP-OES) and by measuring the membrane permeability of the inclusion complexes in home-made two-compartment diffusion cells (Figure S18). Results show the capacity fade rates of 0.117, 0.029, and 0.025% h^{-1} (or 0.037, 0.012, and 0.010% per cycle) were caused by catholyte crossover for Fc⊂HP-β-CD/BTMAP-Vi, HEFc⊂HP-β-CD/BTMAP-Vi and HMFc⊂HP-β-CD/BTMAP-Vi, respectively (Table S7). The remaining capacity loss can therefore be tentatively attributed to the chemical degradation of catholyte. The degradation rates of Fc⊂HP-β-CD, HEFc⊂HP-β-CD, and HMFc⊂HP-β-CD are 0.053, 0.071, and 0.085% h^{-1} (or 0.016, 0.029, and 0.036% per cycle), respectively.

The above results indicate the order of apparent chemical degradation rate for Fc⊂HP-β-CD, HEFc⊂HP-β-CD and HMFc⊂HP-β-CD follow the sequence of Fc⊂HP-β-CD < HEFc⊂HP-β-CD < HMFc⊂HP-β-CD, inversely correlated to the formation constant *K'* (Figure 4a, Figure 2a). Typical ex situ stability measurements suggest the reduced form of the catholyte, for instance, Fc⊂HP-β-CD, remained chemically stable when stored at 65 °C for one week (Figure S19). We observed the change in color and the slow formation of dark brown precipitation for the oxidized form of the catholyte under similar conditions (Figure S20).

Based on ^{1}H NMR spectroscopy, liquid chromatography-mass spectrometry (LC–MS) and X-ray photoelectron spectroscopy (XPS) analyses, we proposed a degradation mechanism for the inclusion complexes, as shown in Figure 4b. The binding between ferrocene derivatives and HP-β-CD is significantly weakened when ferrocene derivatives are electrochemically oxidized (Figure 4a), releasing Fc^+, $HEFc^+$ or $HMFc^+$. They are vulnerable to the nucleophile attack by water or Cl^- and undergo ligand exchange, generating cyclopentadienyl anions and $[Fe(Cp)_m(H_2O)_n]^{(3-m)+}$. The cyclopentadienyl anions could then be oxidized by ferrocenium ions, affording ferrocene derivatives and cyclopentadienyl radicals that tend to polymer-

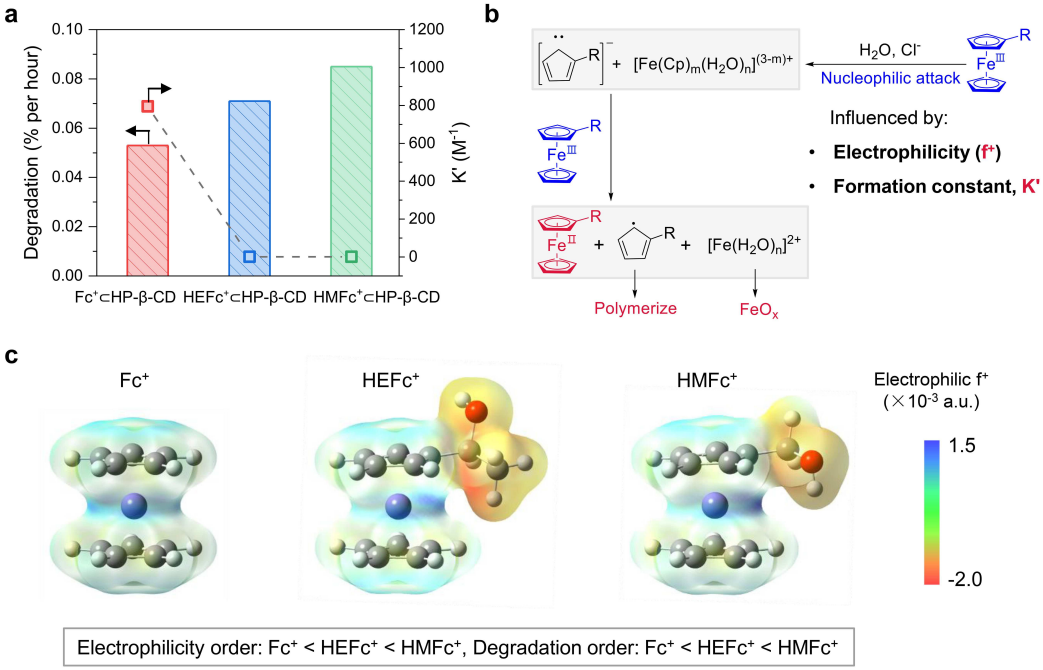

Figure 4. Chemical stability analysis for Fc⊂HP-β-CD, HEFc⊂HP-β-CD, and HMFc⊂HP-β-CD. (a) Chemical degradation rate of Fc⊂HP-β-CD, HEFc⊂HP-β-CD, and HMFc⊂HP-β-CD at 0.1 M, as determined from extended cell cycling experiments by subtracting capacity loss caused by catholyte crossover, and the formation constant of ferrocenium ions with HP-β-CD (*K'*). (b) Schematics showing the degradation mechanism of the inclusion complexes once oxidized. (c) Electrophilic Fukui function (f^+) isosurface of Fc^+, $HEFc^+$, and $HMFc^+$, demonstrating the electrophilicity of the ferrocenium ions.

ize (forming molecules with a molecular weight of less than 1000, Figures S21, S22, and S23). Ferrous oxide is also identified during the process (Figure S24).[14]

We conclude that the apparent chemical degradation of the inclusion complexes during cell cycling was caused by the instability of Fc^+, $HEFc^+$ or $HMFc^+$ under nucleophilic attack and the chemical degradation rate follows the order of $Fc^+ < HEFc^+ < HMFc^+$. The instability caused by nucleophilic attack can be reflected by the different values of electrophilic Fukui function (f^+) and a larger f^+ indicates a greater possibility of nucleophilic attack.[16] As shown in Figure 4c, the Fe^{III} center appears to be the site of nucleophilic attack and the f^+ is in the order of $Fc^+ < HEFc^+ < HMFc^+$, consistent with the order chemical degradation rate. It is worth mentioning that the inclusion of Fc^+ in HP-β-CD may protect it from nucleophilic attack, slowing down the chemical degradation. We speculate that further increase in the stability of oxidized form the Fc⊂HP-β-CD can be accomplished by making the binding between Fc^+ and HP-β-CD stronger.

Improved cycling stability of ferrocene inclusion complexes

According to the chemical stability analysis, Fc⊂HP-β-CD presents the best chemical stability owing to the low electrophilicity of Fc^+ and the binding between Fc^+ and HP-β-CD ($K' = 794.2\ M^{-1}$). Nevertheless, its battery performance is still relatively poor. To further improve its cyclic stability, we employed a lower cutoff voltage of 0.9 V for charge in the Fc⊂HP-β-CD/BTMAP–Vi cell test, while the other conditions are the same as the aforementioned flow cell test. By lowering the charge voltage, the operating SOC was limited and the degradation of oxidized ferrocene derivatives was effectively mitigated. Therefore, we demonstrated the improved cycling stability by more than an order of magnitude, with the capacity fade rate from $0.10\%\,h^{-1}$ (or 0.041% per cycle) to $0.0073\%\,h^{-1}$ (or 0.0020% per cycle) (Figure 5). This capacity fade rate of Fc⊂HP-β-CD is comparable to that of BTMAP-Fc ($0.0014\%\,h^{-1}$ or 0.0011% per cycle).[7b]

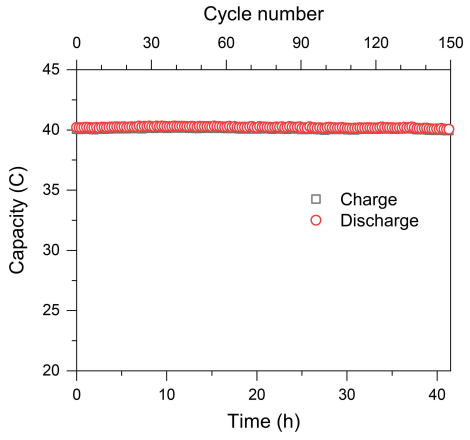

Figure 5. Improved cycling stability of Fc⊂HP-β-CD/BTMAP–Vi cell with a lower cutoff voltage of 0.9 V for charge. The other conditions are the same as those in Figure 3.

Conclusions

We present a strategy that exploits the inclusion of a water-insoluble organic guest in a water-soluble organic host, affording electrochemically active electrolytes for aqueous organic flow batteries (AOFB), exemplified by the host–guest inclusion of ferrocene derivatives in hydroxypropyl-β-cyclodextrin (HP-β-CD). The stability of the inclusion complexes is determined by the binding strength between ferrocene derivatives in HP-β-CD. They undergo a chemical–electrochemical mechanism in cyclic voltammetry studies and show fast redox kinetics and low electron transfer resistance. When adopted in a pH-neutral AOFB as cathode electrolytes, they exhibited a viable battery performance. Our experimental and calculation results imply that the degradation of the inclusion complexes is mainly ascribed to the chemical instability of the ferrocenium ions, which do not combine, or weakly combine, with HP-β-CD, and are vulnerable to nucleophilic attack. By limiting the state of charge, the degradation of ferrocenium ions was mitigated and the improved cycling stability with a capacity fade rate of $0.0073\%\,h^{-1}$ (or 0.0020% per cycle) was demonstrated. Considering the convenience in electrolyte preparation, the strategy we propose here may be broadly applicable, for instance, the host–guest inclusion of viologen derivatives in cucurbiturils, with both the oxidized form and the reduced form forming strongly bound complexes.

Experimental Section

Preparation of inclusion complex electrolytes: Inclusion complex electrolytes were prepared by mixing Fc derivatives and β-CDs together in water. NaCl was added as the supporting electrolyte to increase the conductivity of the solution.

Host–guest interaction characterizations: 2D NMR spectra were acquired in D_2O at 25 °C on a Bruker AVANCE AV400. Isothermal titration calorimetry (ITC) measurements were performed on a MicroCal iTC_{200} and all solutions were prepared in phosphate buffer at a pH of 6.86.

DFT calculations: Dipole moment and electrophilic Fukui function (f^+) was calculated using the Gaussian 16 program at the B3LYP/6-31 + G(d) level.[17] Polarizable Continuum Model was used, and all optimized structures were confirmed by vibrational frequency calculations. The f^+ was analyzed with Multiwfn.[18]

Electrochemical studies: CV studies were carried out under 10 mM ferrocene derivative and 30 mM HP-β-CD in 1 M NaCl solution, on a ZENNIUM E electrochemical workstation (ZAHNER, Germany). Glassy carbon (3 mm diameter), Ag/AgCl, and platinum coil were used as the working electrode, reference electrode, and counter electrode, respectively. RDE measurements were conducted under 1 mM ferrocene derivative and 3 mM HP-β-CD in 1 M NaCl solution, on a CHI600E potentiostat (CH Instruments, Inc., Austin, US) and a Pine E4TQ RDE. Glassy carbon (5 mm diameter), Ag/AgCl, and platinum coil were used as the working electrode, reference electrode, and counter electrode, respectively. LSV scans were recorded at $5\ mV\,s^{-1}$ with a rotating speed in the range of 100–3600 rpm. At each rotating speed, three scans were recorded and averaged to ensure reproducible results. Background scans were also recorded and subtracted.

Solubility measurements: Solubility of β-CDs was measured by adding β-CDs to 5 mL of H_2O until no solid could be further dissolved. The saturated solution was then diluted by a known

ratio, and the concentration was determined by total organic carbon measurements (on Vario TOC). The solubility of β-CD, M-β-CD (r), and HP-β-CD in water are 0.015, 0.79, and 0.83 M, respectively. According to the molar ratio (1:3) at complexation equilibrium, we can obtain the solubility of ferrocene derivatives enabled by the inclusion of HP-β-CD in water is 0.28 M.

Full cell tests: Cell hardware was purchased from Fuel Cell Tech (Albuquerque, US). Selemion DSV membrane was sandwiched between the positive and negative electrodes, which comprised 3 stacked sheets of carbon paper. Both the membrane and electrodes have a geometric area of 5 cm^2. The electrolytes were circulated through the cell stack at a pumping rate of 60 rpm. Polarization curves were acquired by charging the cell to certain SOC, then polarized on a Bio-Logic BCS-815. Potential-controlled electrochemical impedance spectroscopy was recorded at frequencies ranging from 1 Hz to 10 kHz. Galvanostatic cycling at current densities of 10, 20, 40, and 60 mA cm^{-2} was performed with cutoff voltages at 1.1 V for the charge process and at 0.3 V for the discharge process. Prolonged galvanostatic cycling with different cutoff voltage for charge (1.1 or 0.9 V) was conducted at 40 mA cm^{-2}, a potential hold was imposed until the current density fell below 4 mA cm^2.

Catholyte crossover evaluation: Crossover of the inclusion complexes to the anolyte side was estimated through post-cell measurements of ferrocene derivatives with ICP-OES and by measuring the membrane permeability of the inclusion complexes in home-made two-compartment diffusion cells.

Chemical stability experiments: Chemical stability studies were conducted at a neutral pH under 65 °C. Two Fc⊂HP-β-CD samples (0.1 M Fc, 0.3 M HP-β-CD in 1 M NaCl, 2 mL) were prepared. One sample was fully charged in the glovebox. Both samples were strictly degassed, sealed, and transferred into FEP vials, which were stored in an oven at 65 °C for one week and then taken out for ^{1}H NMR spectroscopy, LC–MS and XPS analyses.

Further detailed experimental and computational methods as well as full characterization data are included in the Supporting Information.

Acknowledgements

This project has been supported by the National Natural Science Foundation of China (Nos. 21878281, 21922510, U20A20127, and 21720102003) and the DNL Cooperation Fund, CAS (DNL201910). The numerical calculations were performed on the supercomputing system in the Supercomputing Center at the University of Science and Technology of China.

Conflict of Interest

The authors declare no conflict of interest.

Keywords: aqueous organic flow battery · catholyte · cyclodextrin · ferrocene · host–guest inclusion

[1] B. Obama, *Science* **2017**, *355*, 126–129.
[2] a) G. L. Soloveichik, *Chem. Rev.* **2015**, *115*, 11533–11558; b) J. Winsberg, T. Hagemann, T. Janoschka, M. D. Hager, U. S. Schubert, *Angew. Chem. Int. Ed.* **2017**, *56*, 686–711; *Angew. Chem.* **2017**, *129*, 702–729; c) J. Noack, N. Roznyatovskaya, T. Herr, P. Fischer, *Angew. Chem. Int. Ed.* **2015**, *54*, 9776–9809; *Angew. Chem.* **2015**, *127*, 9912–9947.
[3] a) J. Luo, B. Hu, M. Hu, Y. Zhao, T. L. Liu, *ACS Energy Lett.* **2019**, *4*, 2220–2240; b) D. G. Kwabi, Y. Ji, M. J. Aziz, *Chem. Rev.* **2020**, *120*, 6467–6489; c) F. R. Brushett, M. J. Aziz, K. E. Rodby, *ACS Energy Lett.* **2020**, *5*, 879–884.
[4] a) M. Wu, Y. Jing, A. A. Wong, E. M. Fell, S. Jin, Z. Tang, R. G. Gordon, M. J. Aziz, *Chem* **2020**, *6*, 1432–1442; b) Y. Ji, M. A. Goulet, D. A. Pollack, D. G. Kwabi, S. Jin, D. Porcellinis, E. F. Kerr, R. G. Gordon, M. J. Aziz, *Adv. Energy Mater.* **2019**, *9*, 1900039; c) S. Jin, E. M. Fell, L. Vina-Lopez, Y. Jing, P. W. Michalak, R. G. Gordon, M. J. Aziz, *Adv. Energy Mater.* **2020**, *10*, 2000100.
[5] a) B. Yang, L. Hoober-Burkhardt, F. Wang, G. K. Surya Prakash, S. R. Narayanan, *J. Electrochem. Soc.* **2014**, *161*, A1371-A1380; b) M. Park, E. S. Beh, E. M. Fell, Y. Jing, E. F. Kerr, D. Porcellinis, M. A. Goulet, J. Ryu, A. A. Wong, R. G. Gordon, J. Cho, M. J. Aziz, *Adv. Energy Mater.* **2019**, *0*, 1900694.
[6] N. A. Turner, M. B. Freeman, H. D. Pratt, A. E. Crockett, D. S. Jones, M. R. Anstey, T. M. Anderson, C. M. Bejger, *Chem. Commun.* **2020**, *56*, 2739–2742.
[7] a) B. Hu, C. DeBruler, Z. Rhodes, T. L. Liu, *J. Am. Chem. Soc.* **2017**, *139*, 1207–1214; b) E. S. Beh, D. De Porcellinis, R. L. Gracia, K. T. Xia, R. G. Gordon, M. J. Aziz, *ACS Energy Lett.* **2017**, *2*, 639–644; c) J. Yu, M. Salla, H. Zhang, Y. Ji, F. Zhang, M. Zhou, Q. Wang, *Energy Storage Mater.* **2020**, *29*, 216–222.
[8] a) T. Liu, X. Wei, Z. Nie, V. Sprenkle, W. Wang, *Adv. Energy Mater.* **2016**, *6*, 1501449; b) T. Janoschka, N. Martin, M. D. Hager, U. S. Schubert, *Angew. Chem. Int. Ed.* **2016**, *55*, 14427–14430; *Angew. Chem.* **2016**, *128*, 14639–14643; c) Z. Chang, D. Henkensmeier, R. Chen, *ChemSusChem* **2017**, *10*, 3193–3197; d) J. Winsberg, C. Stolze, A. Schwenke, S. Muench, M. D. Hager, U. S. Schubert, *ACS Energy Lett.* **2017**, *2*, 411–416; e) Y. Liu, M.-A. Goulet, L. Tong, Y. Liu, Y. Ji, L. Wu, R. G. Gordon, M. J. Aziz, Z. Yang, T. Xu, *Chem* **2019**, *5*, 1861–1870.
[9] D. P. Tabor, R. Gómez-Bombarelli, L. Tong, R. G. Gordon, M. J. Aziz, A. Aspuru-Guzik, *J. Mater. Chem. A* **2019**, *7*, 12833–12841.
[10] a) A. Harada, *Acc. Chem. Res.* **2001**, *34*, 456–464; b) S. Wu, Y. Bao, D. Wang, X. Wang, H. Liu, Z. Li, M. Chen, C. Wang, Q. Guo, *J. Mol. Liq.* **2020**, *300*, 112212.
[11] a) L. Peng, A. Feng, M. Huo, J. Yuan, *Chem. Commun.* **2014**, *50*, 13005–13014; b) W. S. Jeon, K. Moon, S. H. Park, H. Chun, Y. H. Ko, J. Y. Lee, E. S. Lee, S. Samal, N. Selvapalam, M. V. Rekharsky, V. Sindelar, D. Sobransingh, Y. Inoue, A. E. Kaifer, K. Kim, *J. Am. Chem. Soc.* **2005**, *127*, 12984–12989.
[12] J. F. Kucharyson, L. Cheng, S. O. Tung, L. A. Curtiss, L. T. Thompson, *J. Mater. Chem. A* **2017**, *5*, 13700–13709.
[13] T. Matsue, D. H. Evans, T. Osa, N. Kobayashi, *J. Am. Chem. Soc.* **1985**, *107*, 3411–3417.
[14] a) R. Prins, A. R. Korswagen, A. G. T. G. Kortbeek, *J. Organomet. Chem.* **1972**, *39*, 335–344; b) G. Tabbì, C. Cassino, G. Cavigiolio, D. Colangelo, A. Ghiglia, I. Viano, D. Osella, *J. Med. Chem.* **2002**, *45*, 5786–5796.
[15] M. A. Goulet, M. J. Aziz, *J. Electrochem. Soc.* **2018**, *165*, A1466-A1477.
[16] B. Wang, C. Rong, P. K. Chattaraj, S. Liu, *Theor. Chem. Acc.* **2019**, *138*, 124.
[17] M. J. Frisch, G. W. Trucks, H. B. Schlegel, G. E. Scuseria, M. A. Robb, J. R. Cheeseman, G. Scalmani, V. Barone, G. A. Petersson, H. Nakatsuji, X. Li, M. Caricato, A. V. Marenich, J. Bloino, B. G. Janesko, R. Gomperts, B. Mennucci, H. P. Hratchian, J. V. Ortiz, A. F. Izmaylov, J. L. Sonnenberg, Williams, F. Ding, F. Lipparini, F. Egidi, J. Goings, B. Peng, A. Petrone, T. Henderson, D. Ranasinghe, V. G. Zakrzewski, J. Gao, N. Rega, G. Zheng, W. Liang, M. Hada, M. Ehara, K. Toyota, R. Fukuda, J. Hasegawa, M. Ishida, T. Nakajima, Y. Honda, O. Kitao, H. Nakai, T. Vreven, K. Throssell, J. A. Montgomery Jr., J. E. Peralta, F. Ogliaro, M. J. Bearpark, J. J. Heyd, E. N. Brothers, K. N. Kudin, V. N. Staroverov, T. A. Keith, R. Kobayashi, J. Normand, K. Raghavachari, A. P. Rendell, J. C. Burant, S. S. Iyengar, J. Tomasi, M. Cossi, J. M. Millam, M. Klene, C. Adamo, R. Cammi, J. W. Ochterski, R. L. Martin, K. Morokuma, O. Farkas, J. B. Foresman, D. J. Fox, Wallingford, CT, **2016**.
[18] T. Lu, F. Chen, *J. Comput. Chem.* **2012**, *33*, 580–592.

Manuscript received: October 28, 2020
Revised manuscript received: November 26, 2020
Accepted manuscript online: December 9, 2020
Version of record online: December 21, 2020

ChemSusChem

Supporting Information

Functioning Water-Insoluble Ferrocenes for Aqueous Organic Flow Battery via Host–Guest Inclusion

Yuanyuan Li[+], Ziang Xu[+], Yahua Liu, Shijian Jin, Eric M. Fell, Baoguo Wang, Roy G. Gordon, Michael J. Aziz, Zhengjin Yang,* and Tongwen Xu*

General information

Ferrocene (Fc), hydroxymethylferrocene (HMFc), carboxylferrocene (CFc), acetylferrocene (AFc), β-cyclodextrin (β-CD), randomly methylated β-cyclodextrin (M-β-CD (r)), hydroxypropyl-β-cyclodextrin (HP-β-CD), sodium chloride (NaCl), and sodium methanesulfonate were purchased from Energy Chemical Co., Ltd. (Shanghai, China). 1-hydroxyethylferrocene (HEFc) was obtained from TCI Chemicals Co., Ltd. (Shanghai, China). Heptakis(2,6-di-O-methyl)-β-cyclodextrin (M-β-CD (D)) was purchased from Acros Organics (New Jersey, USA). Other chemicals were obtained from domestic vendors. Deionized water was used throughout the work.

Host-guest interaction characterizations

2D NMR spectra were acquired in D_2O at 25 °C on a Bruker AVANCE AV400.

Isothermal titration calorimetry (ITC) measurements were performed on a MicroCal iTC_{200}. All solutions were prepared in phosphate buffer at a pH of 6.86. The molecular weights of β-CD and M-β-CD (D) are certain, while an average molecular weight was used for HP-β-CD. The molar changes in Gibbs free energy (ΔG), enthalpy (ΔH) and entropy ($-T\Delta S$) upon complexation process, and the formation constants of β-CDs with ferrocene derivatvies in reduced form were obtained. The formation constants of HP-β-CD with ferroceen derivatives in the oxidized form were calculated from the following equations.

$Fc^+ + [BTMAP\text{-}Vi]^{3+} \rightleftharpoons Fc + [BTMAP\text{-}Vi]^{4+}$ $\Delta G_1 = -nFE_1$

$Fc + HP\text{-}\beta\text{-}CD \rightleftharpoons Fc\subset HP\text{-}\beta\text{-}CD$ $\Delta G_2 = -RT\ln K$

$Fc^+ + HP\text{-}\beta\text{-}CD \rightleftharpoons Fc^+\subset HP\text{-}\beta\text{-}CD$ $\Delta G_3 = -RT\ln K'$

$Fc^+\subset HP\text{-}\beta\text{-}CD + [BTMAP\text{-}Vi]^{3+} \rightleftharpoons Fc\subset HP\text{-}\beta\text{-}CD + [BTMAP\text{-}Vi]^{4+}$ $\Delta G_4 = -nFE_2$

$\Delta G_1 - \Delta G_4 = \Delta G_3 - \Delta G_2$

$-nF(E_1-E_2) = -RT\ln(K'/K)$

$K' = K \exp[nF(E_1-E_2)/RT]$

Where, ΔG is the molar free energy change of the complexation process, n is the number of electrons transferred, E is the cell voltage, K and K' are the formation constants of the complexes in reduced form and the oxidized form, respectively. Faraday's constant F = 96485 J V^{-1} mol^{-1}, ideal gas constant R = 8.314 J K^{-1} mol^{-1}, temperature T = 298.15 K.

Electrochemical studies

Cyclic voltammetry (CV) studies. CV studies were carried out in 1.0 M NaCl aqueous solution, on a ZENNIUM E electrochemical workstation (ZAHNER, Germany). Glassy carbon (3 mm diameter), Ag/AgCl (0.2046 V vs. SHE), and platinum coil were used as the working electrode, reference electrode and counter electrode, respectively. The glassy carbon electrode was polished with alumina slurry (0.5 μm) prior to measurements.

Rotating-disk-electrode (RDE) measurements. RDE measurements were conducted on a

CHI600E potentiostat (CH Instruments, Inc., Austin, US) and a Pine E4TQ RDE. Glassy carbon (5 mm diameter), Ag/AgCl, and platinum coil were used as the working electrode, reference electrode and counter electrode, respectively. Linear sweep voltammetry (LSV) scans were recorded at a scan rate of 5 mV s^{-1} with rotating speed in the range 100-3600 rpm. At each rotating speed, three scans were recorded and averaged to ensure reproducible results. Background scans were also taken and subtracted. A Levich plot of the limiting current vs. the square root of rotating speed was constructed. Diffusion coefficient of the inclusion complexes was calculated from the slope of the linear fitting curve, according to Levich equation: $i=0.620nFAcD^{2/3}v^{-1/6}\omega^{1/2}$, where n = 1, Faraday's constant F = 96485 C mol^{-1}, electrode area A = 0.196 cm^2, molar concentration c = 1×10^{-6} mol cm^{-3}, the kinematic viscosity u = 9.56×10^{-3} cm^2 s^{-1} (1 M NaCl aqueous solution), and D represents the diffusion coefficient. The solution viscosity does not change when adding 3 mM β-CDs.[1] Tafel equation between the kinetic current (i_k) for the oxidation of inclusion complexes and the overpotential (η), $\log_{10}(i_k)=\log_{10}(nFAk_0)+\alpha nF\eta/2.303RT$, was used to deduce the electron transfer rate constant (k_0).

Full cell tests

Cell hardware was purchased from Fuel Cell Tech (Albuquerque, US) and pyrosealed POCO graphite flow plates with serpentine flow fields were used on both sides. The electrode on each side comprised 3 stacked sheets of Sigracet SGL 39AA carbon paper electrodes (with a geometric area of 5 cm^2). Selemion DSV membrane with a thickness of 97 μm was sandwiched between the positive and negative electrodes. The electrolytes were circulated through the cell stack at a pumping rate of 60 rpm. Polarization curves were acquired by charging the cell to certain states of charge (SOCs), then polarized on a Bio-Logic BCS-815. Potential-controlled electrochemical impedance spectroscopy was recorded as needed at frequencies ranging from 1 Hz to 10 kHz. Galvanostatic cycling at current densities of 10, 20, 40, and 60 mA cm^{-2} was performed with cutoff voltages at 1.1 V for the charge process and at 0.3 V for the discharge process. Prolonged galvanostatic cycling with potential holds until the current density fell below 4 mA cm^2 was conducted at 40 mA cm^{-2}.

Permeability measurements

The permeation of the inclusion complex electrolytes across a Selemion DSV membrane was evaluated with a lab-made two-compartment diffusion cell. The donating side comprises 0.1 M Fc⊂HP-β-CD, HMFc⊂HP-β-CD or HEFc⊂HP-β-CD aqueous solution, whereas the receiving side comprises a same volume of 0.15 M NaCl aqueous solution, which balanced the ionic strengths and minimized the effect of osmotic pressure. The solutions in both compartments were vigorously agitated during the course. Samples were collected from the receiving side every 12 h, analyzed by UV-vis spectrometer (TU-1901), and then poured back. The permeability (P) was calculated from the following equation:

$$P=\frac{\ln(1-\frac{2C_r}{C_0})(-\frac{Vl}{2A})}{t}$$

where C_r is the concentration measured at the receiving reservoir, C_0 is the active species concentration in the donating reservoir (0.1 M), V is the volume of the receiving side (15 mL), l

is the membrane thickness (97 μm), A is the membrane area (1.89 cm^2), and t is time. The permeability of BTMAP-Vi has been measured and published in a previous report.[2]

Capacity loss caused by catholyte crossover

Crossover of the inclusion complexes to the anolyte side was estimated through post-cell measurements with inductively coupled plasma-optical emission spectrometry (ICP-OES). For the 0.1 M Fc⊂HP-β-CD/BTMAP-Vi cell, the capacity loss per hour attributed to permeation Q_{perm}, is calculated as follows.

$$Q_{perm}^{Fc\subset HP\text{-}\beta\text{-}CD}=Fn_{perm}=F\frac{C_aV_a}{t_{total}}$$

$$=96485\times\frac{1.06\times10^{-5}\times11}{108.51}\ \text{C/h}=0.104\ \text{C/h}$$

Where, F is Faraday's constant, C_a is the concentration of Fc⊂HP-β-CD in anolyte, V_a is the volume of anolyte, t_{total} is the total time of full cell tests.

The total capacity loss per hour is:

$$Q_{total}=\frac{88.29\text{-}74.25}{108.51\text{-}15.32}\ \text{C/h}=0.151\ \text{C/h}$$

The percentage of capacity loss attributed to crossover per cycle is:

$$\frac{Q_{perm}^{Fc\subset HP\text{-}\beta\text{-}CD}}{Q_{total}}\times100\%=\frac{0.104}{0.151}\times100\%=68.9\%$$

Similarly, we calcualted the percentage for HMFc⊂HP-β-CD/BTMAP-Vi and HEFc⊂HP-β-CD/BTMAP-Vi cell to be 22.9% and 28.7%, respectively.

Chemical stability experiments

Chemical stability studies were conducted at a neutral pH under 65 °C. Two Fc⊂HP-β-CD samples (0.1 M Fc, 0.3 M HP-β-CD in 1 M NaCl, 2 mL) were prepared. One sample was fully charged in the glovebox. Both samples were strictly degassed, sealed and transferred into FEP vials, which were stored in an oven at 65 °C for one week and then taken out for characterization.

No obvious change was noticed for the pristine sample after heating at 65 °C for one week (**Figure S19**). However, color of charged sample changed from dark blue into light yellow, with dark brown precipitation formed after the sample being heated at 65 °C. ^{1}H NMR spectra showed new peaks (**Figure S20 and S21**). The charged sample after heat treatment was extracted with $CDCl_3$ and the extractions were characterized by ^{1}H NMR (**Figure S22**). A new bulk peak indicated that the decomposition product was mainly Fc. Other small, broad peaks implied the existence of oligomers, which were further tested by liquid chromatography-mass spectrometry (LC-MS) on a Bruker microTOF-Q II mass spectrometer (**Figure S23**). The precipitation of heated sample in the charged stated was washed three times with 10 mL of deionized water and acetone, respectively, and then evenly spread on a piece of silicon slice for X-ray photoelectron spectroscopy (XPS) detection performed on a Thermo ESCALAB MK

II instrument (**Figure S24**). The obtained spectrum matches ferrous oxide.[3] We conclude that Fc⊂HP-β-CD in reduced form is chemically stable, while the charged/oxidized form is easy to decompose.

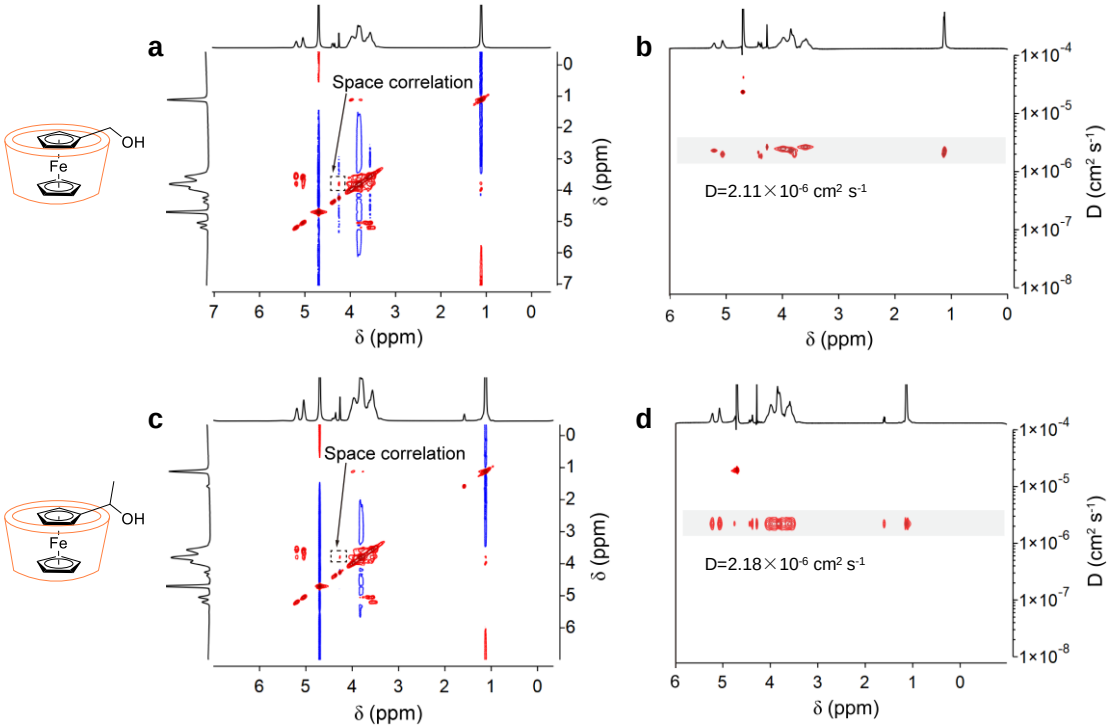

Figure S1. The two dimensional NOESY and DOSY spectra showing the host-guest interaction between HMFc (a, b) or HEFc (c, d) and HP-β-CD. D is the diffusion coefficient as determined from the DOSY spectra. The dashed boxes highlight the space correlation.

Figure S2. Photos of heterogeneous solutions of CFc⊂HP-β-CD and AFc⊂HP-β-CD. Precipitations can be clearly seen at the bottom of the vials.

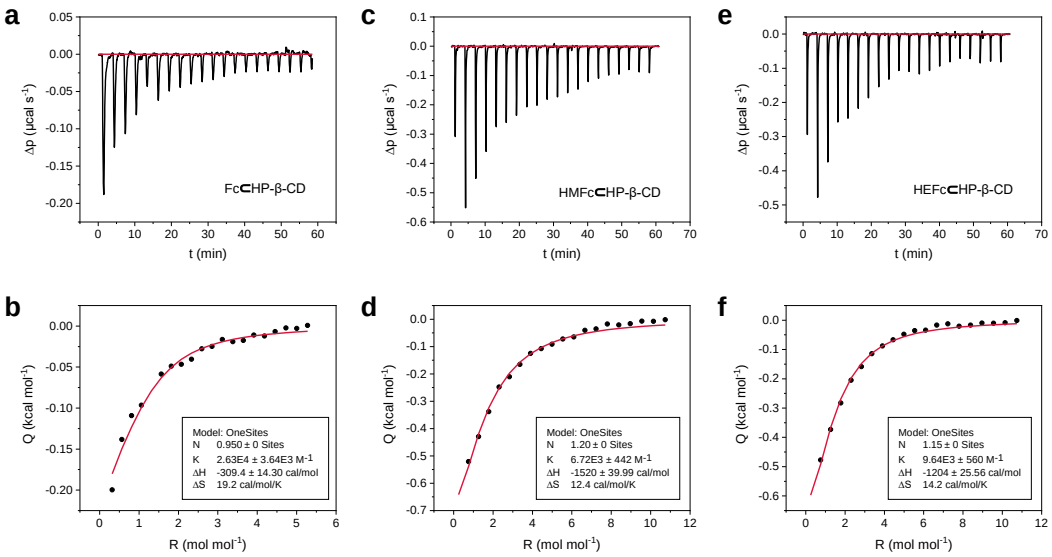

Figure S3. Isothermal titration calorimetry (ITC) measurements for the formation of the inclusion complexes between ferrocene derivatives and HP-β-CD. Raw thermograms (a, c, e) depict the differential heating power versus time and isotherms (b, d, f) show the integrated and normalized reaction heat as a function of the molar ratio of HP-β-CD to ferrocene derivatives.

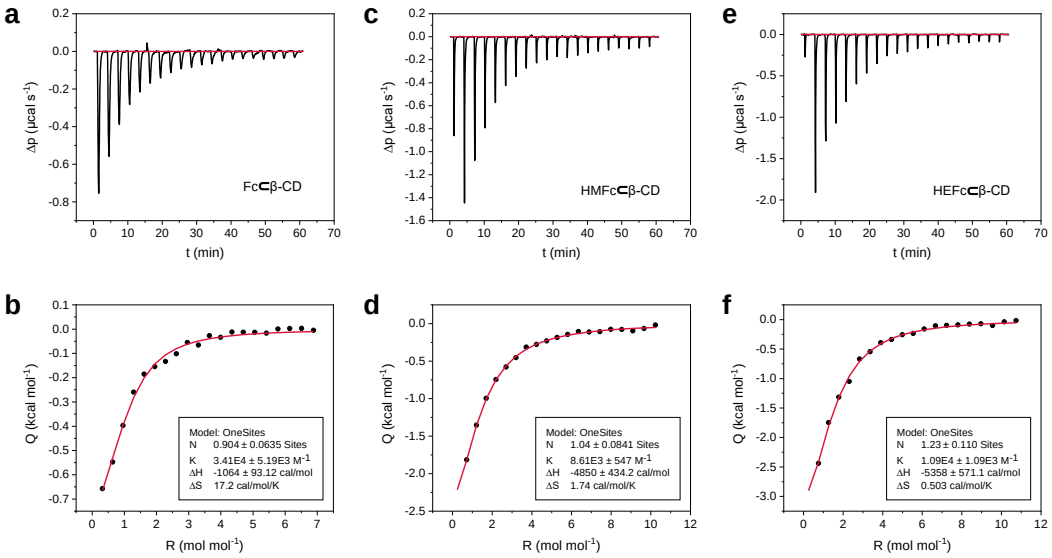

Figure S4. Isothermal titration calorimetry (ITC) measurements for the formation of the inclusion complexes between ferrocene derivatives and β-CD. Raw thermograms (a, c, e) depict the differential heating power versus time and isotherms (b, d, f) show the integrated and normalized reaction heat as a function of the molar ratio of β-CD to ferrocene derivatives.

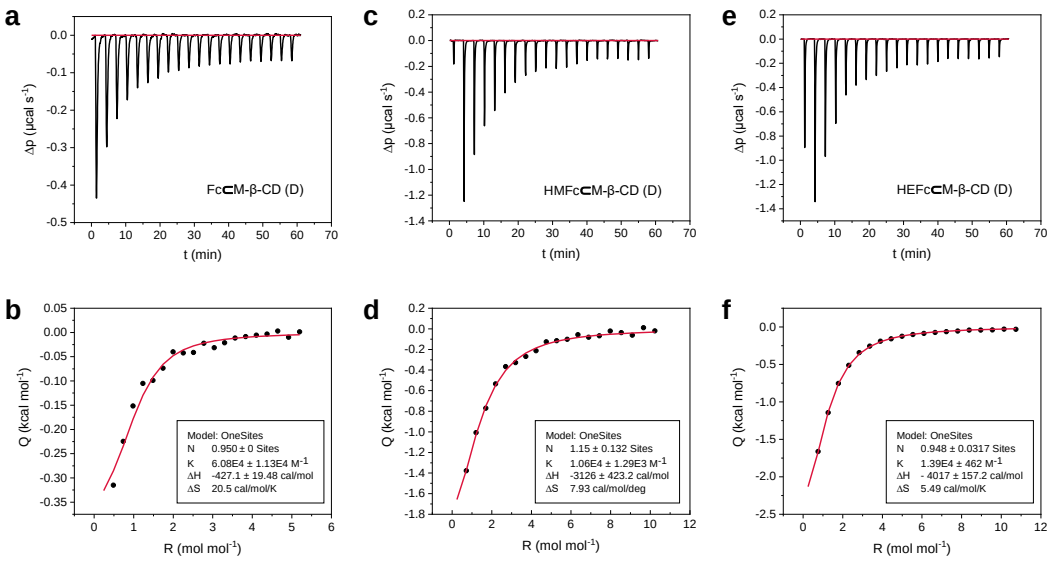

Figure S5. Isothermal titration calorimetry (ITC) measurements for the formation of the inclusion complexes between ferrocene derivatives and M-β-CD (D). Raw thermograms (a, c, e) depict the differential heating power versus time and isotherms (b, d, f) show the integrated and normalized reaction heat as a function of the molar ratio of M-β-CD (D) to ferrocene derivatives.

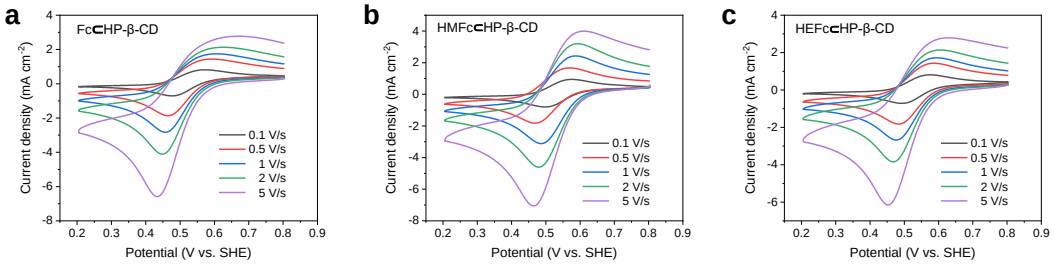

Figure S6. Cyclic voltammograms of (a) Fc⊂HP-β-CD, (b) HMFc⊂HP-β-CD and (c) HEFc⊂HP-β-CD recorded at 10 mM in 1 M NaCl supporting electrolyte at varied potential sweeping rates. Potential was referenced to standard hydrogen electrode (SHE). The molar ratio of ferrocene derivatives to HP-β-CD is 1:3.

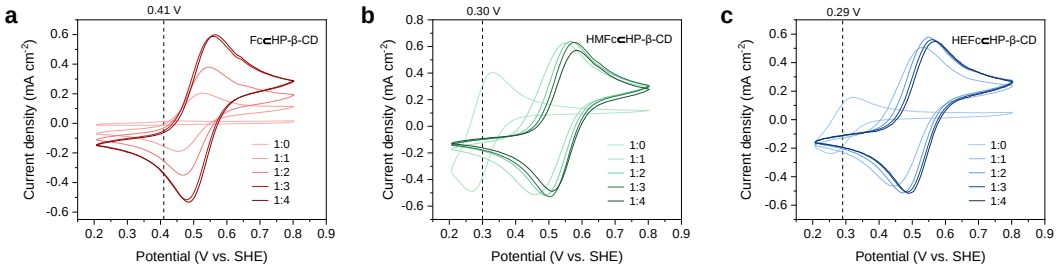

Figure S7. Cyclic voltammograms of 10 mM of (a) Fc, (b) HMFc and (c) HEFc recorded at 50 mV/s in 1 M NaCl supporting electrolyte, by adding various portions of HP-β-CD. Potential was referenced to standard hydrogen electrode (SHE).

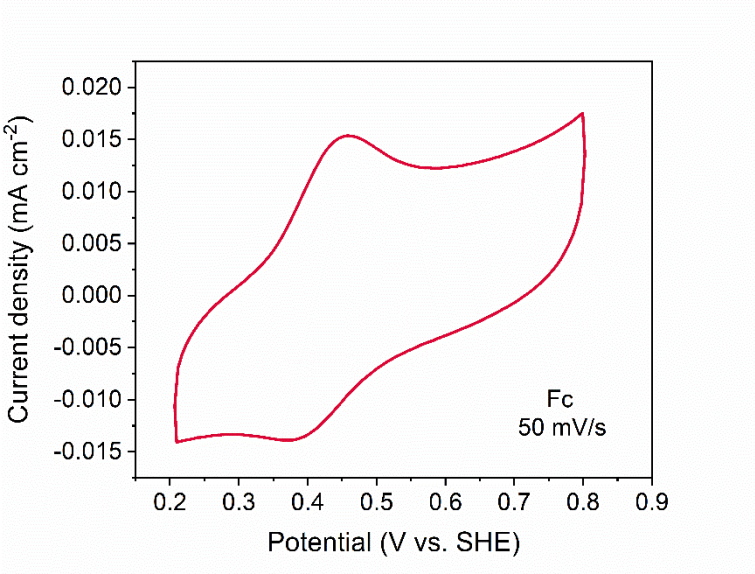

Figure S8. Cyclic voltammogram of 10 mM Fc recorded at 50mV/s in 1 M NaCl solution. Potential was referenced to standard hydrogen electrode (SHE).

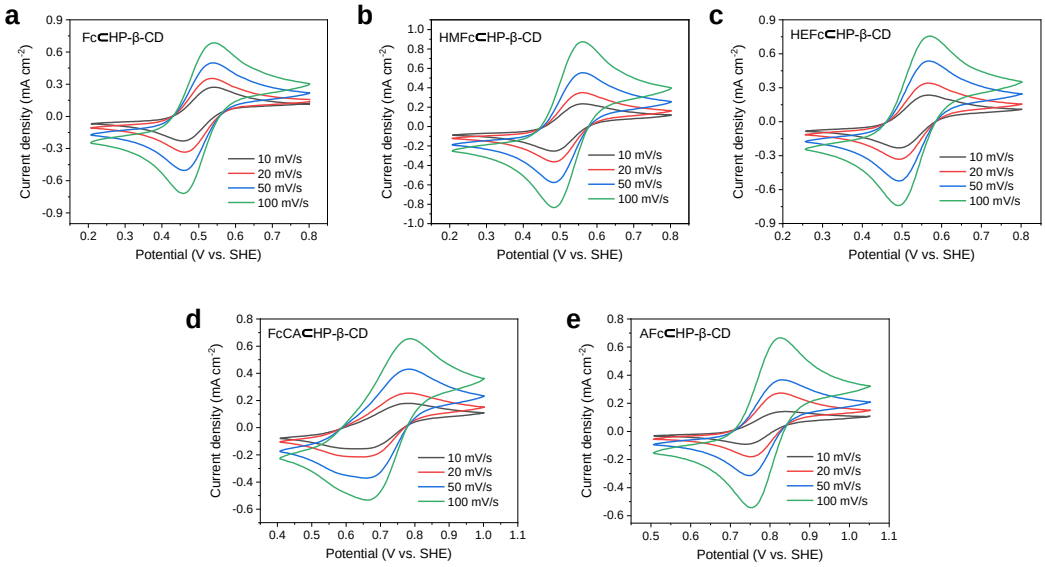

Figure S9. Cyclic voltammograms of 10 mM of (a) Fc⊂HP-β-CD, (b) HMFc⊂HP-β-CD, (c) HEFc⊂HP-β-CD, (d) FcCA⊂HP-β-CD and (e) AFc⊂HP-β-CD in 1 M NaCl solution at various potential scanning rates. Potential was referenced to standard hydrogen electrode (SHE). The molar ratio of ferrocene derivatives to HP-β-CD is 1:3.

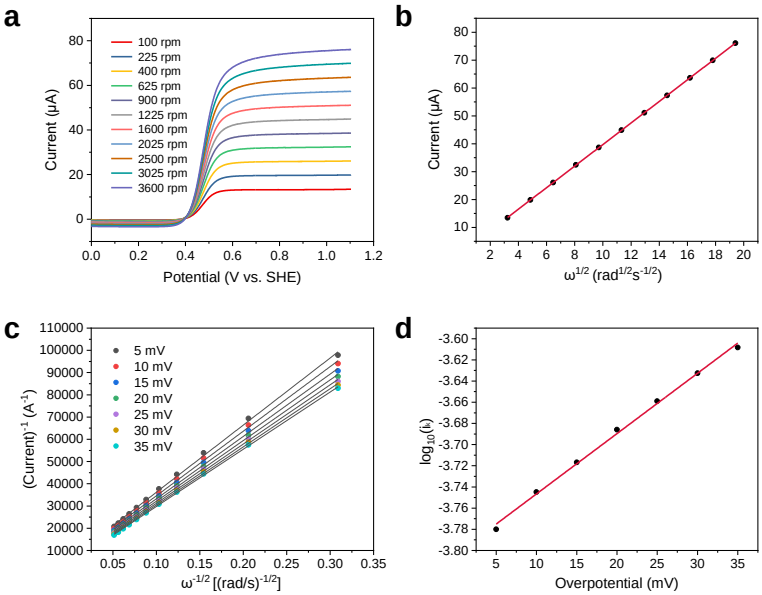

Figure S10. Rotating-disk-electrode experiment on Fc⊂HP-β-CD (molar ratio 1:3, 1 mM in 1 M NaCl). (a) Current versus potential at different rotating rates with a potential scanning rate of 5 mV s^{-1}. (b) Levich plot of limiting current versus the square root of rotating rate ($\omega^{1/2}$). (c) Koutecky–Levich plot at different over-potentials (potential deviation from the formal reduction potential, referenced to SHE). (d) Tafel plot, the logarithm of kinetically limited current versus over-potential.

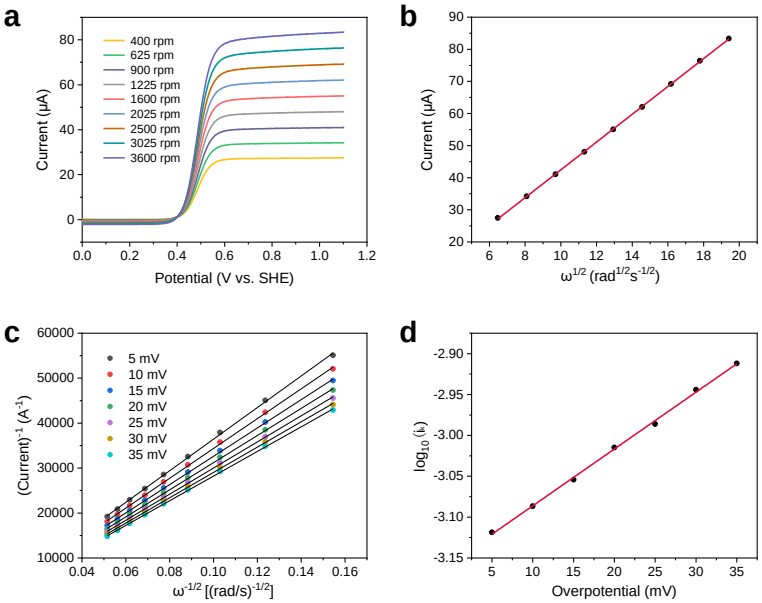

Figure S11. Rotating-disk-electrode experiment on HMFc⊂HP-β-CD (molar ratio 1:3, 1 mM in 1 M NaCl). (a) Current versus potential at different rotating rates with a potential scanning rate of 5 mV s^{-1}. (b) Levich plot of limiting current versus the square root of rotating rate ($\omega^{1/2}$). (c) Koutecky–Levich plot at different over-potentials (potential deviation from the formal reduction potential, referenced to SHE). (d) Tafel plot, the logarithm of kinetically limited current versus over-potential.

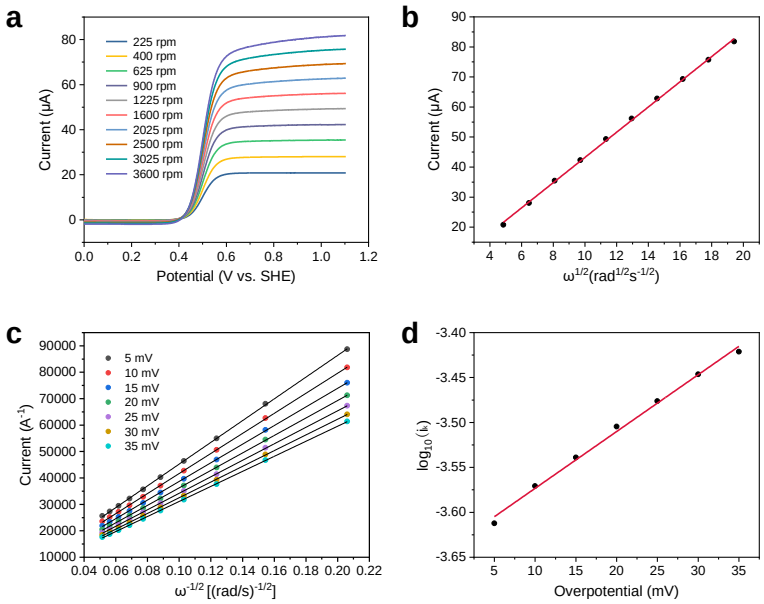

Figure S12. Rotating-disk-electrode experiment on HEFc⊂HP-β-CD (molar ratio 1:3, 1 mM in 1 M NaCl). (a) Current versus potential at different rotating rates with a potential scanning rate of 5 mV s^{-1}. (b) Levich plot of limiting current versus the square root of rotating rate ($\omega^{1/2}$). (c) Koutecky–Levich plot at different over-potentials (potential deviation from the formal reduction potential, referenced to SHE). (d) Tafel plot, the logarithm of kinetically limited current versus over-potential.

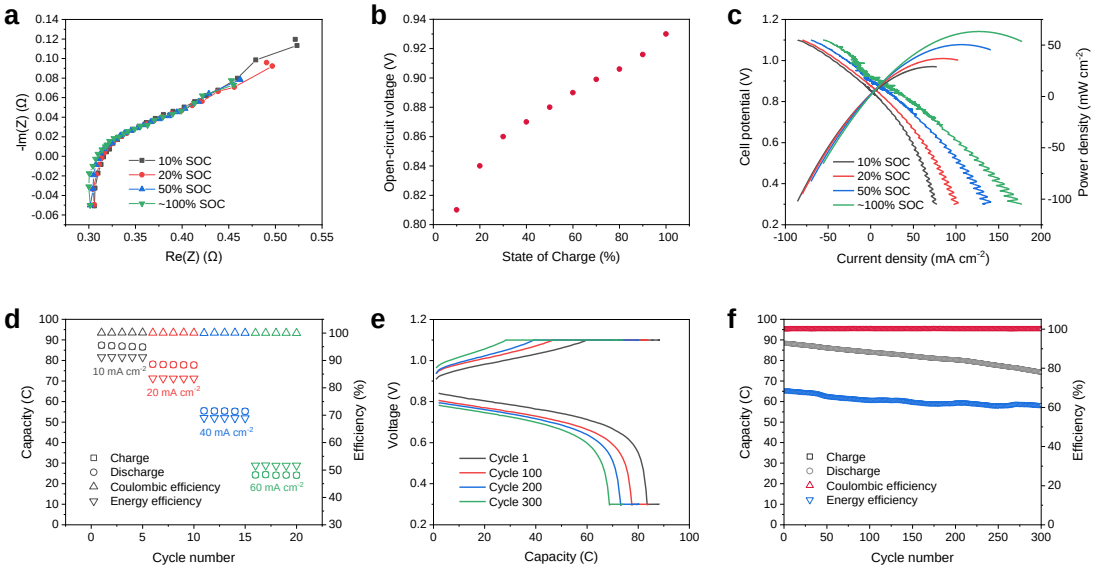

Figure S13. Performance of a neutral-pH AOFB assembled with Fc⊂HP-β-CD (0.1 M) in the catholyte (10 mL) and BTMAP-Vi (0.1 M) in anolyte (15 mL, 1.5 times e^- excess). (a) Electrochemical impedance spectroscopy (EIS) at varied SOCs. (b) Open-circuit-voltage versus SOC. (c) Polarization curves recorded at varied SOCs. (d) Charge-discharge capacity, CE, and EE at current densities of 10, 20, 40, and 60 mA cm^{-2}, respectively. (e, f) Long-term galvanostatic cycling with potential holds at 40 mA cm^{-2}. Charge-discharge capacity, EE and CE were plotted as functions of the cycle number.

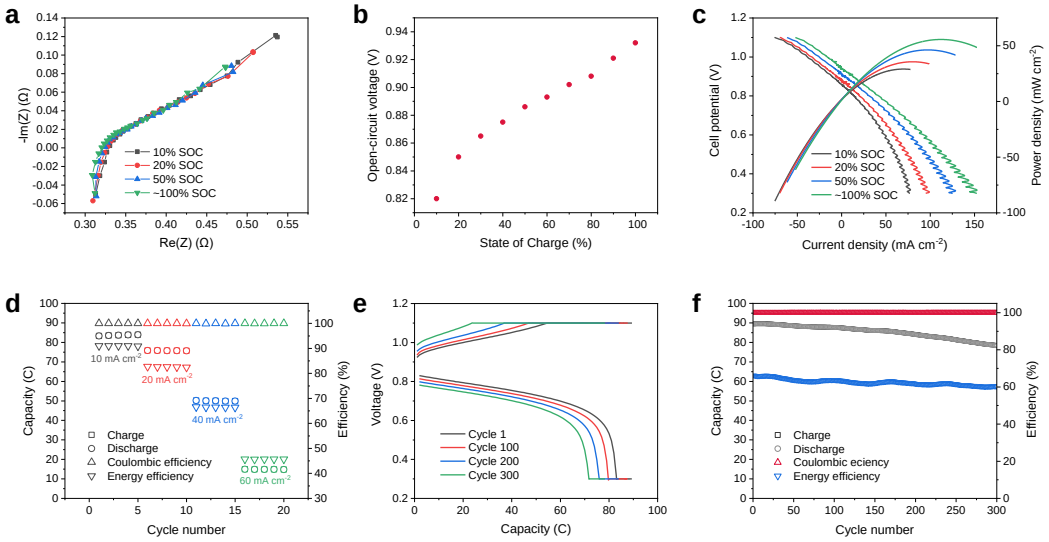

Figure S14. Performance of a neutral-pH AOFB assembled with HEFc⊂HP-β-CD (0.1 M) in the catholyte (10 mL) and BTMAP-Vi (0.1 M) in anolyte (15 mL, 1.5 times e^- excess). (a) Electrochemical impedance spectroscopy (EIS) at varied SOCs. (b) Open-circuit-voltage versus SOC. (c) Polarization curves recorded at varied SOCs. (d) Charge-discharge capacity, CE, and EE at current densities of 10, 20, 40, and 60 mA cm^{-2}, respectively. (e, f) Long-term galvanostatic cycling with potential holds at 40 mA cm^{-2}. Charge-discharge capacity, EE and CE were plotted as functions of the cycle number.

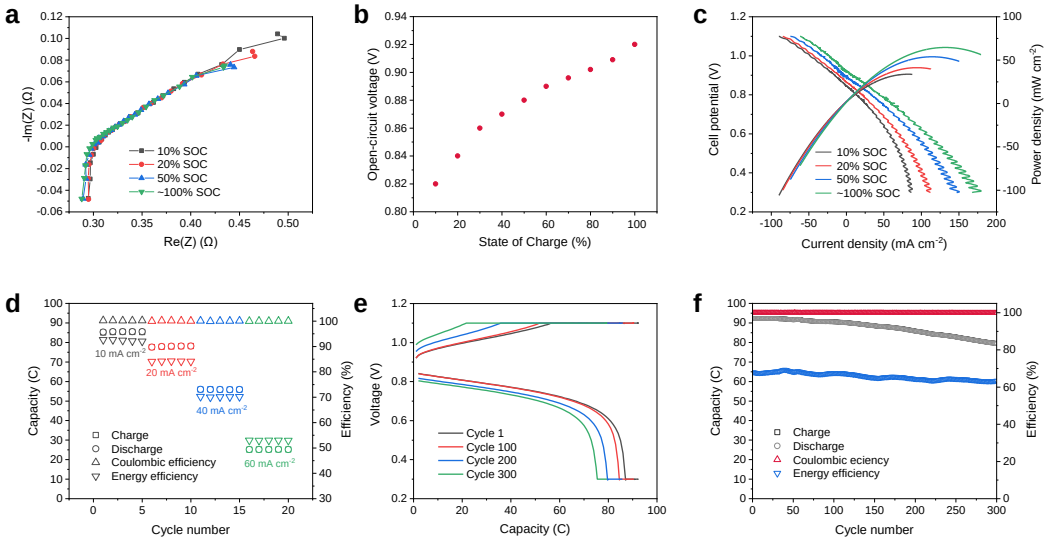

Figure S15. Performance of a neutral-pH AOFB assembled with HMFc⊂HP-β-CD (0.1 M) in the catholyte (10 mL) and BTMAP-Vi (0.1 M) in anolyte (15 mL, 1.5 times e^- excess). (a) Electrochemical impedance spectroscopy (EIS) at varied SOCs. (b) Open-circuit-voltage versus SOC. (c) Polarization curves recorded at varied SOCs. (d) Charge-discharge capacity, CE, and EE at current densities of 10, 20, 40, and 60 mA cm^{-2}, respectively. (e, f) Long-term galvanostatic cycling with potential holds at 40 mA cm^{-2}. Charge-discharge capacity, EE and CE were plotted as functions of the cycle number.

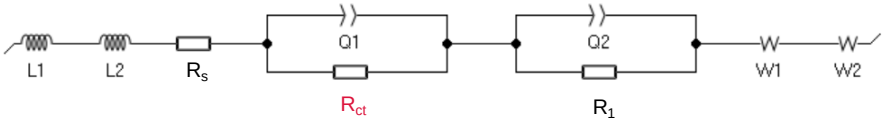

Figure S16. Equivalent circuit for the electrochemical impedance spectroscopy (EIS) fitting.

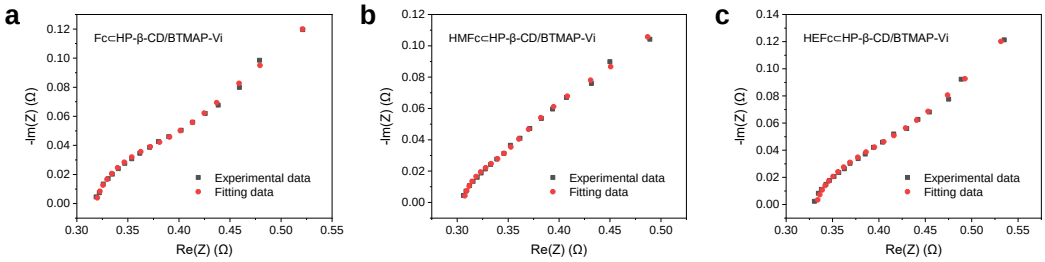

Figure S17. Experimental and fitted EIS spectra of the pH-neutral AOFBs assembled with the inclusion complexes.

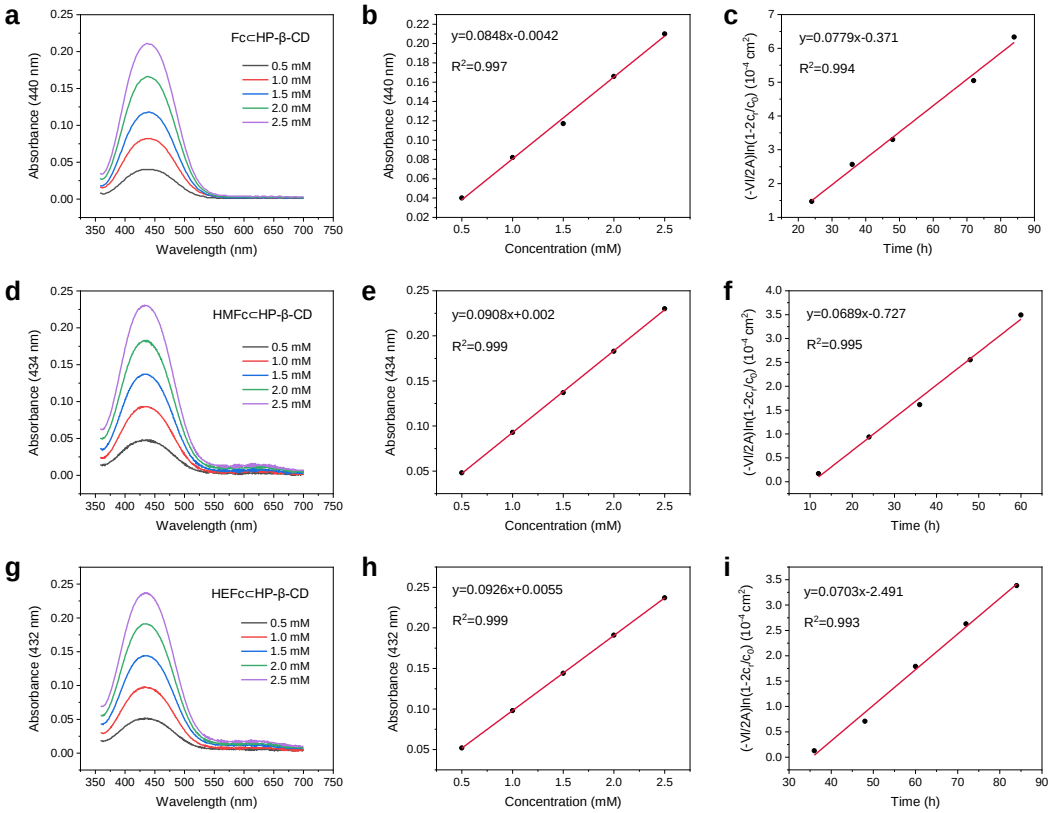

Figure S18. (a, d, g) UV-Vis spectra of the inclusion complexes at known concentrations. (b, e, h) The absorbance as a function of concentrations at the maximum absorption wavelength. (c, f, i) Normalized concentration of receiving side as a function of time. Permeability values as determined from the slope of the curves are 2.16×10^{-9} cm^2 s^{-1}, 1.91×10^{-9} cm^2 s^{-1} and 1.95×10^{-9} cm^2 s^{-1} for FcCHP-β-CD, HMFcCHP-β-CD and HEFcCHP-β-CD, respectively.

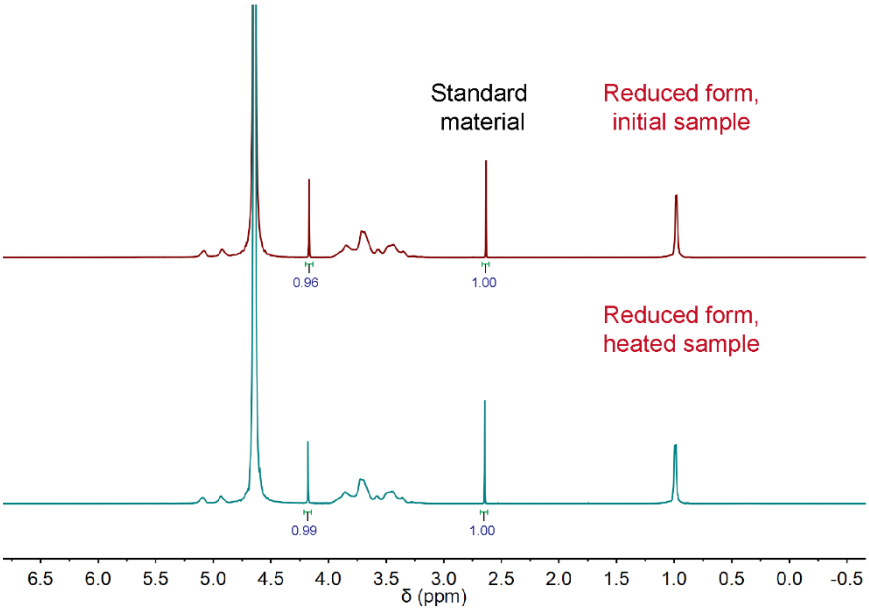

Figure S19. ^{1}H NMR spectra of Fc⊂HP-β-CD heated at 65 °C for one week (bottom) compared with that from the initial sample (top).

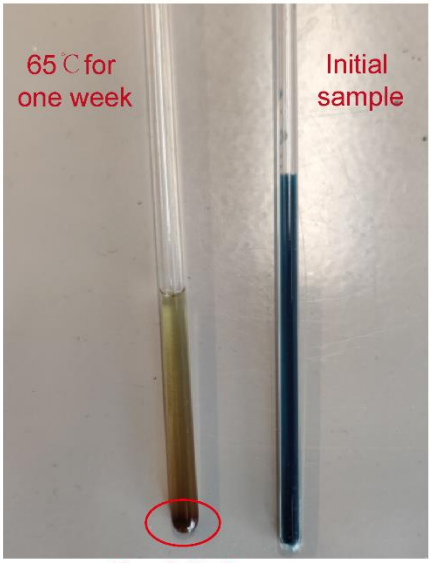

Figure S20. Photograph of the heated (left) and the initial (right) Fc^{+}⊂HP-β-CD sample.

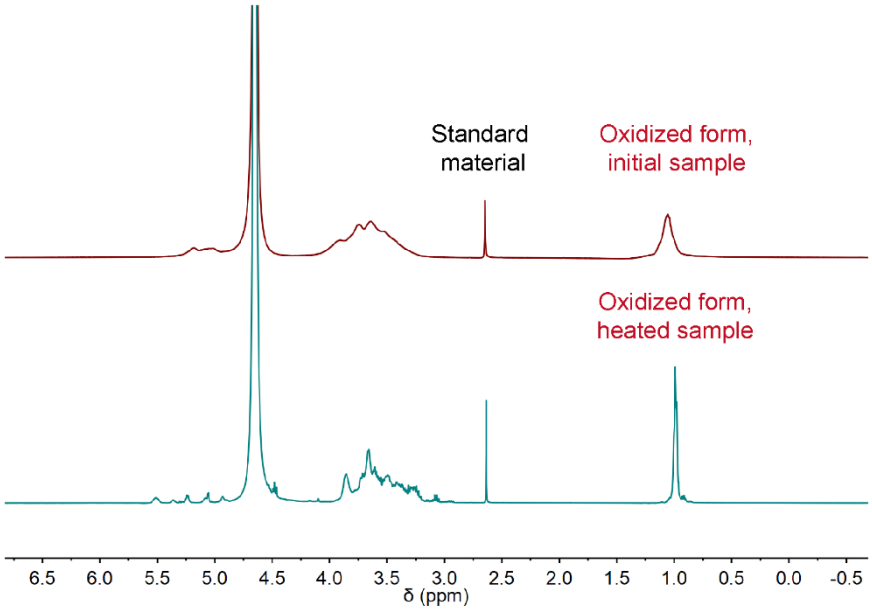

Figure S21. ^{1}H NMR spectra of Fc^{+}⊂HP-β-CD heated at 65 °C for one week (bottom), compared with that of the initial sample (top).

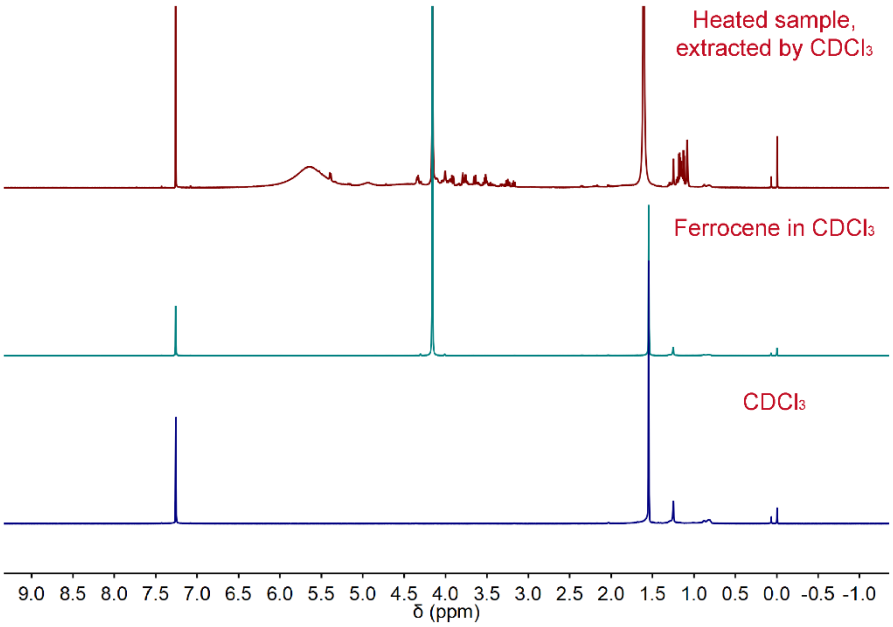

Figure S22. ^{1}H NMR spectra of $CDCl_3$ (bottom), ferrocene dissolved in $CDCl_3$ (middle), and extractions of the charged sample after heat treatment with $CDCl_3$ (top).

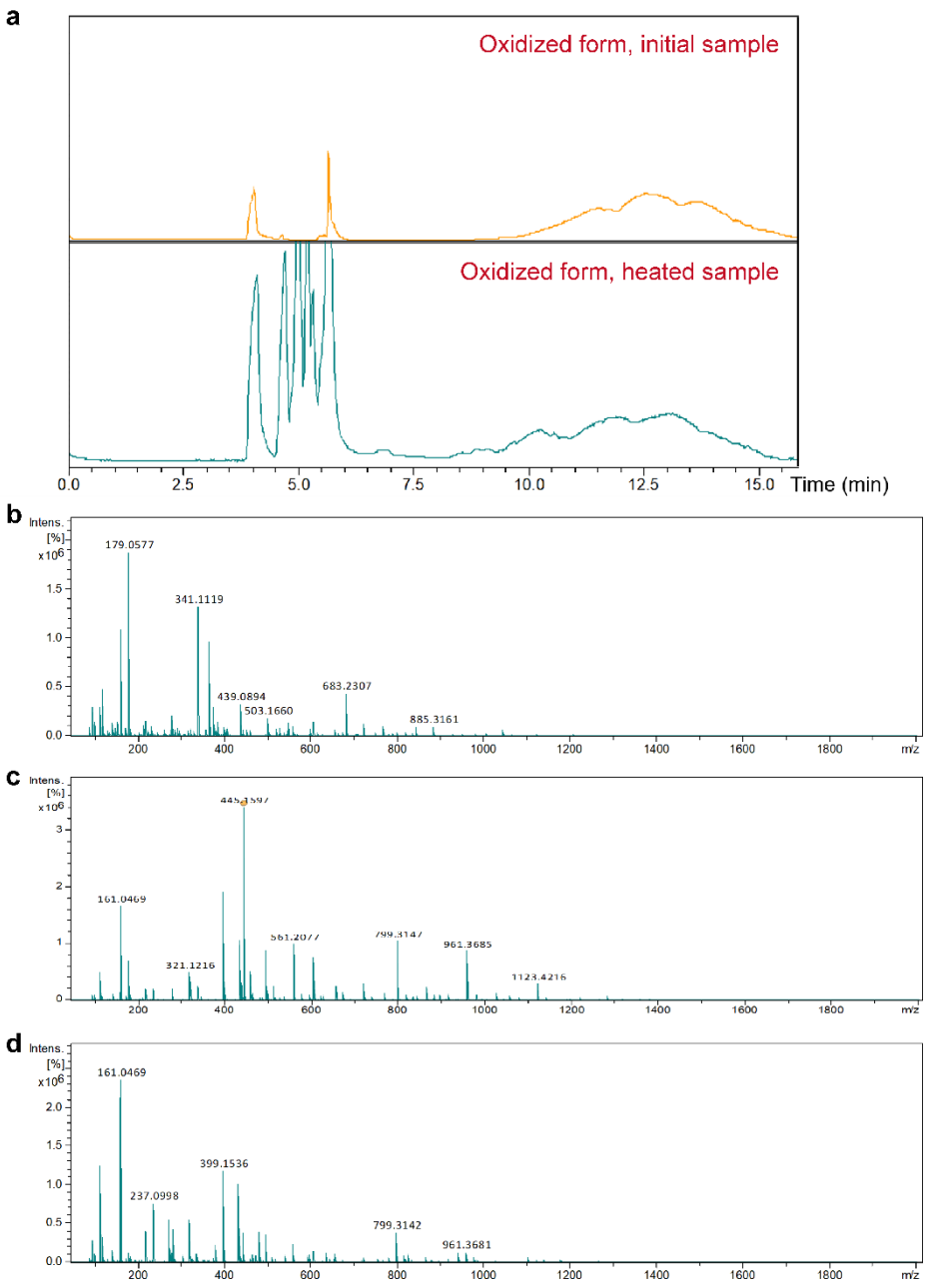

Figure S23. (a) High resolution LC-MS spectra of the charged catholyte sample (top) and of the charged sample being heated under 65°C for one week (bottom) showing the appearance of three new peaks at a retention time of ~5 min. (b,c, d) Mass spectrum of the material eluted at around 5 min as the 1st, 2nd and 3rd peak.

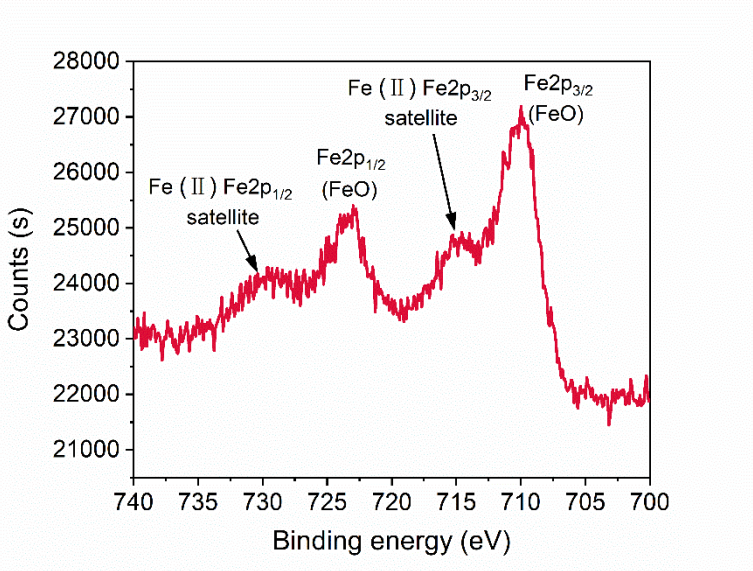

Figure S24. XPS spectra of thoroughly washed precipitations generated in the charged sample after being treated at 65 °C for one week.

Table S1. Dipole moment of ferrocene derivative obtained from DFT calculations.

Species	Fc	HMFc	HEFc	CFc/CFc^{-}	AFc
Dipole moment (Debye)	0.002	2.59	2.43	3.49/16.28	5.16

Table S2. Thermodynamic parameters characterizing the complexation of ferrocene derivatives with β-cyclodextrin obtained by ITC at 25 °C.

Species	ΔH (cal mol^{-1})	-TΔS (cal mol^{-1})	ΔG (cal mol^{-1})	K (×10^3 M^{-1})	N
Fc⊂β-CD	-1064	-5042.18	-6106.18	34.1	0.904
HMFc⊂β-CD	-4850	-518.78	-5368.78	8.61	1.04
HEFc⊂β-CD	-5358	-137.39	-5495.39	10.9	1.23
Fc⊂M-β-CD (D)	-427.1	-6112.08	-6539.18	60.8	0.950
HMFc⊂M-β-CD (D)	-3126	-2364.33	-5490.33	10.6	1.15
HEFc⊂M-β-CD (D)	-4017	-1636.84	-5653.84	13.9	0.950
Fc⊂HP-β-CD	-309.4	-5724.48	-6033.88	26.3	0.950
HMFc⊂HP-β-CD	-1520	-3309.47	-5217.06	6.72	1.20
HEFc⊂HP-β-CD	-1204	-4233.73	-5437.73	9.64	1.15

Table S3. Water solubility at 25 °C and price of β-CDs.

Species	Water Solubility (M)	Price ($ kg^{-1})
β-CD	0.015	56
M-β-CD (D)	-	28995
M-β-CD (r)	0.79	1377
HP-β-CD	0.83	112

Price of β-CDs are quoted from the website ⟨www.energy-chemical.com/front/index.htm⟩.

Table S4. Formation constants of HP-β-CD with ferrocene derivatives in reduced form (K) and the oxidized form (K'), respectively.

Species	K (M^{-1})	K' (M^{-1})
Fc	26300	794.19
HMFc	6720	1.28
HEFc	9640	0.85

Table S5. Electrochemical properties of Fc⊂HP-β-CD, HMFc⊂HP-β-CD, HEFc⊂HP-β-CD, and previously reported ferrocene-based electrolytes.

Electrolyte	$E_{1/2}$ (V vs SHE)	ΔE (mV)	D ($cm^2\ s^{-1}$)	k_0 ($cm\ s^{-1}$)	Reference
Fc (in DMF)	0.56	127	8.9×10^{-6}	1.4×10^{-2}	[4]
FcNCl	0.62	68	3.74×10^{-6}	3.66×10^{-5}	[5]
FcN_2Br_2	0.62	64	3.64×10^{-6}	4.60×10^{-6}	[5]
BTMAP-Fc	0.39	71	3.1×10^{-6}	1.4×10^{-2}	[2]
Fc-SO_3Na	0.33	87	3.17×10^{-6}	1.06×10^{-2}	[6]
Fc⊂HP-β-CD	0.50	80	1.87×10^{-6}	8.31×10^{-3}	This work
HMFc⊂HP-β-CD	0.52	74	2.22×10^{-6}	3.70×10^{-2}	This work
HEFc⊂HP-β-CD	0.53	78	2.12×10^{-6}	1.22×10^{-2}	This work

Abbreviations are as follows: $E_{1/2}$, redox potential; ΔE, peak separation between the oxidation and the reduction peak; D, diffusion coefficient; k_0, electron-transfer rate constant.

Table S6. Total cell resistance (R), membrane resistance (R_s), electron transfer resistance (R_{ct}) of the inclusion complex and the peak power density at ~100% state of charge.

Cell	R (Ω cm^2)	R_s (Ω cm^2)	R_{ct} (Ω cm^2)	R_{ct}/R (%)	Peak power density (mW cm^{-2})
Fc⊂HP-β-CD/BTMAP-Vi	2.04	1.55	0.24	11.8	66.22
HMFc⊂HP-β-CD/BTMAP-Vi	1.91	1.51	0.16	8.4	68.55
HEFc⊂HP-β-CD/BTMAP-Vi	2.45	1.62	0.21	8.6	58.16

Table S7. The total capacity loss per hour and those contributed by crossover and chemical degradation of the inclusion complexes.

Cell	Crossover (%/h)	Degradation (%/h)	Total (%/h)
Fc⊂HP-β-CD/BTMAP-Vi	0.117	0.053	0.17
HMFc⊂HP-β-CD/BTMAP-Vi	0.025	0.085	0.11
HEFc⊂HP-β-CD/BTMAP-Vi	0.029	0.071	0.10

References

[1] T. Matsue, D. H. Evans, T. Osa, N. Kobayashi, *J. Am. Chem. Soc.* **1985**, *107*, 3411-3417.

[2] E. S. Beh, D. De Porcellinis, R. L. Gracia, K. T. Xia, R. G. Gordon, M. J. Aziz, *ACS Energy Lett.* **2017**, *2*, 639-644.

[3] a) N. S. McIntyre, D. G. Zetaruk, *Anal. Chem.* **1977**, *49*, 1521-1529; b) A. N. Mansour, R. A. Brizzolara, *Surf. Sci. Spectra* **1996**, *4*, 345-350.

[4] Y. Zhao, Y. Ding, J. Song, G. Li, G. Dong, J. B. Goodenough, G. Yu, *Angew. Chem. Int. Ed.* **2014**, *126*, 11216-11220.

[5] B. Hu, C. DeBruler, Z. Rhodes, T. L. Liu, *J. Am. Chem. Soc.* **2017**, *139*, 1207-1214.

[6] J. Yu, M. Salla, H. Zhang, Y. Ji, F. Zhang, M. Zhou, Q. Wang, *Energy Storage Mater.* **2020**, *29*, 216-222.